2-20-2018

A detailed hydrodynamic study to help community based resiliency planning under extreme climatic and weather events

Md. Golam Rabbani Fahad
Rowan University

A DETAILED HYDRODYNAMIC STUDY TO HELP COMMUNITY BASED RESILIENCY PLANNING UNDER EXTREME CLIMATIC AND WEATHER EVENTS

by

Md Golam Rabbani Fahad

A Thesis

Submitted to the
Department of Civil and Environmental Engineering
College of Engineering
In partial fulfillment of the requirement
For the degree of
Master of Science in Civil Engineering
at
Rowan University
December 1, 2017

Thesis Chair: Dr. Rouzbeh Nazari, Ph.D.

Dedications

I would like to dedicate this manuscript to my parents, Abdul Mazid and Rahima Akhtar Rina.

Acknowledgments

I would like to express my appreciation to Professor Dr. Rouzbeh Nazari for his guidance and help throughout this research. The skills and knowledge that I have gained are things that I will take with me into my next professional endeavor. I look forward to whatever challenges that come my way knowing that I am prepared to take them on.

I would like to thank my wife for her unwavering love and support through this endeavor.

This work was supported through New Jersey Department of Community Affairs (NJDCA) from Superstorm Sandy Community Development Block Grant Disaster Recovery (CDBG-DR). We also acknowledge the World Climate Research Programme's Working Group on Coupled Modelling, which is responsible for CMIP. For CMIP the U.S. Department of Energy's Program for Climate Model Diagnosis and Intercomparison provides coordinating support and led development of software infrastructure in partnership with the Global Organization for Earth System Science Portals.

Abstract

Md Golam Rabbani Fahad
A DETAILED HYDRODYNAMIC STUDY TO HELP COMMUNITY BASED RESILIENCY PLANNING UNDER EXTREME CLIMATIC AND WEATHER EVENTS
2017-2018
Dr. Rouzbeh Nazari, Ph.D.
Master of Science in Civil Engineering

The State of New Jersey is particularly vulnerable to extreme weather and climatic events. This study concentrates on spatial and temporal vulnerability of these events using climate and hydrodynamic modelling. The first chapter focuses on historical climatic trend of temperature and precipitation as well as the future scenarios using 10 bias corrected climate model output considering high end emission scenario derived from Coupled Model Intercomparison Project Phase 5 (CMIP5). In the second chapter a coastal hydrodynamic model called ADCIRC-2DDI was implemented to assess the impact of hurricanes in the Western North Atlantic (WNAT) model domain. The efficiency of the model in representing the complex interaction between storm-tide was assessed considering hurricane SANDY as a historical event. Multiple scenarios were also created to assess the impact of different categories of hurricane for Atlantic City, NJ. The last chapter deals with the inland flooding during extreme storm event. A 2D hydrodynamic model based on Shallow Water Equation (SWE) called TUFLOW was implemented to identify the dynamic spatial and temporal extent of inland flooding. Results from the TUFLOW were coupled with a traffic micro-simulation model to help emergency evacuation planning to help the vulnerable communities with decision making process.

Table of Contents

Table of Contents (Continued)

Table of Contents (Continued)

List of Figures

List of Tables

Chapter 1

Abstract

The complex hydrologic and atmospheric dynamics of New Jersey, along with the prevailing risks of extreme weather events like floods, place this region in particular at a higher risk to the impacts of climate change. The objective of this study is to assess the spatial and temporal change in temperature and precipitation pattern over New Jersey. A multi-model ensemble provides useful information about the uncertainty of the changes of future climate. High emission scenarios using Representative Concentration Pathways (RCP8.5) of the 5th Phase Coupled Model Inter-comparison Project (CMIP5) in the Intergovernmental Panel on Climate Change (IPCC) also aids to capture the possible extremity of climate change. Using the CMIP5 regional climate modeling predictions, this study analyzes the distribution of temperature and precipitation over New Jersey, USA in recent years (1971–2000) and in three future periods (2010-2040, 2041-2070 and 2070-2100) considering RCP 8.5 scenarios. Climate changes are expressed in terms of 30-yr return values of annual near-surface temperature and 24-h precipitation amounts. At the end of the century, the mean temperature increase over New Jersey is expected to increase between 3.5°C to 7.6°C with an increase in total precipitation ranging from 6% to 10%. Spatial analysis showed that the Northern and Western part of New Jersey will experience greater change in temperature and precipitation in the future. Analysis from extreme climate indicators suggests increase in yearly total and high intensity rainfall up to 21st century.

1.1 Introduction

Global change of atmospheric temperature and precipitation patterns can have an adverse impact on both natural and human systems (Hao et al. 2008; Gebre and Ludwig 2015). Climate change possess a great threat to the components of natural system such as sea ice, polar ice, coral reefs, tropical and mangrove forests, wetlands etc. Variability in future climate will increase the risks of extinction of vulnerable species by changing their natural habitat and loss of biodiversity. The human systems sensitive to climate change include mainly water resources, food and agricultural security, marine system, human settlement, energy as well as human health.

Analysis of observed data showed a 0.6°C increase in average global temperature since the late 19th century. The 5th assessment report from IPCC (IPCC-AR5) also projected the potential for temperature rises of up to 4.8°C and sea level rise of up to 0.82 m by 2100 (Stocker 2014). Potential impacts at the local and regional scale are a key concern to the scientific community. Changing climate at regional scales affect fundamental aspects of our life, including health and welfare, economy, and natural ecosystems. Evaluation of climate change is needed at a much higher spatial and temporal resolution for accurate impact assessment (Doherty et al. 2003; Tsvetsinskaya et al. 2003; Kueppers et al. 2005; Hayhoe et al. 2008). Effects of climate change at the global scale are already occurring in the forms of sea-ice loss, sea level rise, acute heat waves, etc. The state of New Jersey, USA lies along the east coast and the threat of sea level rise makes this state vulnerable to future climate change scenarios. Climate change will aggravate events such as flooding, storm damage, and intense heat or cold waves which in turn will lead to detrimental effects upon the increasing population and

infrastructure development. Thus, impact assessment based on climate change has increased significance for a vulnerable region like New Jersey.

General Circulation Models (GCMs) which simulates physical processes in the atmosphere, ocean and land surface considering the response of the global climate system due to increasing greenhouse gas concentrations. A fully coupled atmospheric-ocean general circulation model (AOGCM) comprises of an atmospheric GCM (AGCM) and an ocean GCM (OGCM). GCM depicts the global climate and has a horizontal resolution between 250 and 1000 km. The complexity of the GCMs and need for long term ensemble scenarios result in high computing cost. To avoid that, GCMs usually adopt relatively coarse resolution grid spacing which result in inappropriate representation of topography and local climate (Bhaskaran et al. 2012; Maraun et al. 2010). Various hydrological processes such as radiation, convection, cloud microphysics etc. occur mainly on a finer scale. Due to GCMs coarse resolution, it does not provide full representation of the actual regional climate scenario required for impact analysis. Therefore, downscaling the coarse resolution GCM variables to regional scale is essential for better representation of regional climate (Xu et al. 2005; Fowler et al. 2007). Among two techniques of downscaling the climate variables from GCMs i.e. statistical and dynamical (Wilby and Wigley 1997), the statistical downscaling techniques focus on developing quantitative relationships between atmospheric variables of coarse resolution and finer regional resolution (Wilby et al., 2004). In contrast, dynamic downscaling method uses regional climate models (RCMs) that are developed based on the same principles of dynamical and physical processes as GCMs but with a much finer resolution (10-50 km) that better capture the regional climate (Christensen et al. 2007). Thus,

embedding fine resolution RCMs within GCMs has become a common practice in climate change studies. Previous studies concluded that RCMs significantly improves the model formulation of precipitation, one of the most important climatic variable (Frei et al. 2006; Buonomo et al. 2007).

In recent decades, climate models have continued to be developed and improved significantly. Standard protocols of numerical experiments for climate models were developed in the 3rd Phase of the Coupled Model Intercomparison Project (CMIP3) by the Working Group on Coupled Modelling (WGCM) in response to a proposed activity of the World Climate Research Programme (WCRP) (Meehl et al. 2007). Climate model outputs from the CMIP3 project provided significant contributions to the formation of Fourth Assessment report (AR4) under the Intergovernmental Panel on Climate Change, IPCC (Solomon et al. 2007). IPCC-AR4 is based on emission scenarios which is the basis for conducting climate simulations by external forcing (Meehl et al. 2007). To evaluate the previous model simulations and understand the factors behind the differences in model projections, the 5th phase of the Coupled Model Intercomparison Project (CMIP5) was developed by considering radiative forcing due to greenhouse gas concentration (Taylor et al. 2012). Experiments conducted through CMIP5 multi-model ensemble contributed to the 5th Assessment Report (AR5) (Stocker et al. 2014). Hereafter, outputs from these two projects are named as CMIP3 and CMIP5 datasets. Improved general circulation models from CMIP5 produce better simulation of the AOGCMs and provides better representation of surface air temperature and precipitation distribution than CMIP3 (Stocker et al. 2014). Rammig et al. (2010) concluded CMIP3 lacks certain biogeochemical aspects which lead to even more uncertainty in CMIP3 models.

According to Sperber et al. (2013) CMIP5 models are more skillful at capturing various aspects of Asian monsoon climate than the CMIP3 models. Ogata et al. (2014) and Watterson et al. (2014) also reported modest improvements in climate simulations by CMIP5 models, suggesting an advantage of using CMIP5 model outputs. CMIP5 provides four new future projection scenarios i.e. RCP2.6, RCP4.5, RCP6, and RCP8.5 based on Representative Concentration Pathways (RCPs). RCP 8.5 represents a future with higher emissions and is distinguished by the highest amount of greenhouse gas concentrations up to 21st century (Riahi et al., 2007). However, among the four RCP scenarios, RCP8.5 can reflect the highest possible change in climate. Peters et al. (2013) concluded that the current global emissions tracking scenarios that lead to the highest temperature increases. Considering this fact another study over China was also conducted using the RCP8.5 scenario (Zou and Zhou 2013) that showed increase in total and extreme precipitation over China and Tibetan Plateau. The rest of the pathways are marked as moderate mitigation scenarios as they manifest milder future carbon emissions.

However, systematic errors in climate models typically observed due to erroneous conceptualization, limited spatial resolution, and improper knowledge of climate system process and during spatial averaging of grid cells (Teutschbein and Seibert, 2010). Underrepresentation of existing physio-geographical characteristics results in a serious bias in crucial parameters such as temperature and precipitation (Lucarini et al., 2008; Christensen et al., 2008). Therefore, bias correction of the climate model outputs for hydrologic impact assessment is essential (Wood et al. 2004; Ines and Hansen 2006; Teutschbein and Seibert 2012). Several bias correction procedures such as delta and

scaling approach (Graham et al. 2007), quantile mapping (Seguí et al. 2010), merging of linear and nonlinear empirical-statistical (Themeßl et al. 2011) have been recently used for correcting the climate model outputs to resolve this issue.

The objectives of this paper were to evaluate the (1) current trend of New Jersey's climate, (2) possible high end changes of future climate over for the three future periods i.e. near future (2010-2040), mid future (2041-2070) and far future (2071-2100) and (3) extreme climate indicators over New Jersey. This paper comprises of four main sections and a conclusion. Section one describes the region of study, the digital geographical models that encompass it, and the sources of climate data used. Section two includes a basic analysis of the precipitation and temperature dataset in terms of the integrity of temporal series and the spatial densities of the ground network. Section three is a description of the variability of precipitation and an assessment of orography. Finally, the conclusions compile the main findings.

1.2 Study Site and Methods

1.2.1 Description of the study area. New Jersey (NJ) is in the Mid-Atlantic Region of the Unites States with geographical coordinates between 38°56′ N to 41°21′ N and 73°54′ W to 75°34′ W. It is bordered on the east by the Atlantic Ocean, on the west by the Delaware River and Pennsylvania, on the south by the Delaware Bay, and on the north by the state of New York. Despite its small size, NJ has three distinct climate zones: Northern, Southern, and Coastal (Source: http://climate.rutgers.edu) as shown in Figure 1.

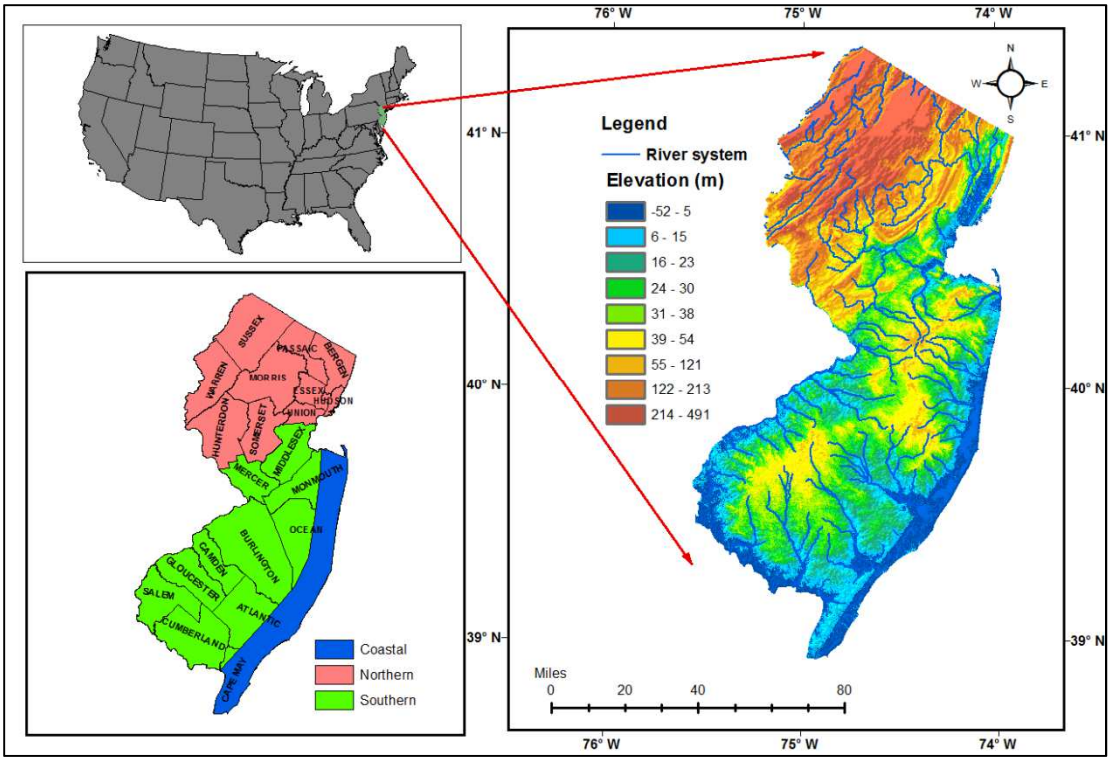

Figure 1. Topography, admin boundary and river system of New Jersey.

The Northern climate zone is part of the Appalachian Uplands and consists of elevated highlands and valleys with a continental climate (Ludlum 1983). The upper Northern zone is mainly comprised of urban areas. These urbanized areas contain impervious surfaces which lead to localized warmer regions known as "urban heat island" effect (Rosenzweig et al. 2005). The Southeast part contains the Pine Barren region with relatively low temperatures due to the pine and oak forests, as well as the porous sandy soils that greatly impact the hydrology of this region. The porous sandy soil permits the precipitation to infiltrate rapidly and during the drier condition higher daily maximum temperature could be a threat to forest fire in this region (Kenneth and Zampella 1987). The Southwest zone is around 30 m above sea level and its close

proximity to the Delaware Bay adds maritime significance to the climate of this region. Finally, the Coastal zone temperature is split between continental and Coastal influences on seasonal and sub-seasonal bases due to the high heat capacity of the adjacent Atlantic Ocean. This region tends to be warmer than other areas during the fall and early winter, but cooler during the spring. Strong humid subtropical climate is dominant in most of the Northern and Northeastern part of the state. The summer season is hot and humid with average temperatures of 28-31°C across the state. During winter average high temperatures remain between 1 to 6°C and lows of -9 to -2°C for most of the state (Robinson 2005). However, wide variations in temperature, along with lower humidity than summer, are the main characteristics of spring and fall seasons. The highest historical extreme temperature was recorded as 43°C on July 10, 1936 and the lowest recorded temperature was -37°C on January 5, 1904 for New Jersey (Ludlum 1983). Precipitation is uniformly distributed through the year with an average annual precipitation ranging from 1100 mm to 1300 mm (Source: http://climate.rutgers.edu/stateclim_v1/nclimdiv/). The 'nor'easters' which is named because of the direction of strongest winds rotating counterclockwise and tends to blow to northeast to southwest (Davis et al. 1993) , a notable feature in New Jersey climate during winter and early spring, causes blizzards and flooding. Hurricanes and tropical storms are quite common in the Mid-Atlantic regions which include New Jersey. Hurricane Sandy (Oct 29, 2012), Irene (Aug 29, 2011) and remnants of Hurricane Katrina (Aug 29, 2005) are some most notable hurricanes that have affected New Jersey in recent years.

1.2.2 Climate data. Trend analysis was conducted over New Jersey's three regional parts (Northern, Southern and Coastal) using the observed data obtained from National Centre for Environmental Information (NCEI) climate database (https://www.ncei.noaa.gov/) for the period of 1900-2010.

Table 1

List of climate models used in the study

GCM	Driving RCM	Resolution	Citation
GFDL-ESM2M	N/A	0.44° (~50 km)	Dunne et al. (2012)
HADGEM2-ES	N/A	0.44° (~50 km)	Jones et al. (2011)
IPSL-CM5A-LR	N/A	0.44° (~50 km)	Dufresne et al. (2013)
MIROC-ESM-CHEM	N/A	0.44° (~50 km)	Watanabe et al. (2011)
NorESM1-M	N/A	0.44° (~50 km)	Bentsen et al. (2013)
GFDL-ESM2M	REGCM4	0.44° (~50 km)	Dunne et al. (2012), Giorgi et al. (2012)
GFDL-ESM2M	WRF	0.44° (~50 km)	Dunne et al. (2012), Skamarock et al. (2005)
HADGEM2-ES	REGCM4	0.44° (~50 km)	Jones et al. (2011), Giorgi et al. (2012)
MPI-ESM-LR	REGCM4	0.44° (~50 km)	Stevens et al. (2013), Giorgi et al. (2012)
MPI-ESM-LR	WRF	0.44° (~50 km)	Stevens et al. (2013), Skamarock et al. (2005)

Climatic variables used in analysis included daily precipitation, average temperature, maximum temperature, and minimum temperature. For future climate analysis, statistically downscaled 5 GCMs and dynamically downscaled 5 RCMs were used. All the products were bias corrected before further analysis. The origin of the climate models used in this study and there related resolutions are provided in Table 1. The GCM products were bias corrected according to the methodology described in Hempel et al. (2013). Bias corrected GCM products were obtained from the inter-sectoral impact model intercomparison project (ISI–MIP) (Warszawski et al. 2014).

Table 2

Description of the RCP scenarios (Collins et al. 2013)

Name	Radiative Forcing	Concentration
RCP8.5	>8.5 W/m^2 in 2100	1370 CO_2-eq
RCP6	6 W/m^2 at stabilization after 2100	850 CO_2-eq at stabilization after 2100
RCP4.5	4.5 W/m^2 at stabilization after 2100	650 CO_2-eq at stabilization after 2100
RCP3-PD (RCP2.6)	Peak at 3 W/m^2 before 2100 and then decline to 2.6 W/m^2	Peak at 490 CO_2-eq before 2100 and then decline

The bias correction procedure applied to the RCM products has been described in McGinnis et al. (2015). Bias corrected RCM products were obtained from the North American CORDEX (NA-CORDEX) server (https://na-cordex.org/). All the climate model data were divided into two parts, (1) historical period (1971-2005) and (2) future RCP 8.5 scenario (2006-2100). Among the four RCPs as shown in Table 2, the high emission scenario RCP 8.5 was chosen for the study. Two climatic variables- average temperature and precipitation were used to assess the climate change impact. Four time slices were considered to represent the possible changes in temperature and precipitation. These time slices are baseline 1970s (1971-2000), early era 2020s (2011-2040), mid era 2050s (2041-2070) and long term era 2080s (2071-2100). To validate the accuracy of the bias corrected climate products over New Jersey the climate model data in the historical period (1971-2000) were compared with the hybrid dataset of Watch Forcing Data-WFD (Weedon et al. 2011) and the Watch Forcing Data methodology applied to ERA-Interim Data (WFDEI) used in the Inter-Sectoral Impact Model Integration and Intercomparison Project ISI-MIP (Weedon et al. 2014) which combines forcing data of WFD (1901-1978) and WFDEI.GPCC (1979-2012). Only the RCP 8.5 scenario was used since it has the most extreme climate forcing such as greenhouse gas concentration as described in IPCC-AR5. Furthermore, it was necessary to match the spatial scale of gridded observed data with model simulated data. The gridded WFD-WFDEI data was interpolated to match the exact grid for the model simulated GCM and RCM products by using Climate Data Operator (CDO) (Schulzweida et al. 2006). Bilinear interpolation was used to regrid purpose because it is computationally faster and smoothing in both horizontal and vertical direction improves the accuracy more than the linear interpolation technique. The spatial

distribution of future temperature and precipitation were produced using inverse distance weighting (IDW) (Bartier et al. 1996). IDW is based on the assumption that the correlation rate and similarities between neighbors is an inverse function of every points from neighboring points. The main advantage of IDW over other interpolation method such as kriging is that it is easy to define thus results are easy to understand and it is less sensitive to outliers than kriging interpolation techniques (Krivoruchko 2011). The average temperature for the period of 1971-2000 (historical period) were first calculated over the study area. Next, average for the three future period (2010-2040, 2041-2070, 2071-2100) were also calculated individually. After that the individual averaged values were subtracted from the historical period to find the spatial pattern of future temperature over New Jersey.

1.2.3 Mann-Kendal test and Sen's slope estimator. We preformed the Mann Kendall (M-K) trend test or 'Kendall t test' (Kendall et al. 1948), which is a widely used non-parametric trend test in climatologic and hydrologic time series. Non-conformity to any particular distribution and low sensitivity to sudden changes due to inhomogeneous data series make this test superior than other trend detection statistics (Önöz and Bayazit 2003). M-K trend test is based on two hypotheses. First the null hypothesis, H_0, assumes that there is no trend, therefore, the data is independent and randomly ordered. The alternative hypothesis, H_1, assumes that the data series follows a monotonic trend. We state whether results of M-K test were significant at different confidence intervals i.e. 99.9%, 99%, 95%, and 90% confidence levels. M-K test only provides the idea of having a trend in data series, so to get a quantitative sense of the increasing or decreasing rate of

that trend, we used the Sen's slope estimator test. (Sen et al. 1968; Gilbert et al. 1987). The slope estimator (S) of the data x is expressed as below:

$$S = \text{median}(y) \tag{1.1}$$

$$y = \frac{x_i - x_j}{i - j} \tag{1.2}$$

Where, $i = 1, 2, 3 \ldots N$ and $i < j$

1.2.4 Climate extreme indicators. The definitions of four extreme climate indicators analyzed in this study are listed in Table 3.

Table 3

List of extreme climate indicators used in this study

Indicators	Description	Definitions	Unit
CDD	Consecutive dry days	Maximum number of consecutive days with RR<1mm	days
CWD	Consecutive wet days	Maximum number of consecutive days with RR≥1mm	days
R95p	Precipitation on very wet days	Annual total rainfall when rainfall >95th percentile	mm
PRCPTOT	Annual total wet-day precipitation	Annual total PRCP in wet days (RR>=1mm)	mm

These indicators were chosen for their strong relevance to various hydrologic events such as high intensity rainfall, flash flood, droughts as well as relevance to ecological processes. The broad and diverse effects of climate change of ecological process includes alteration in carbon cycle, life cycle and growth of microorganisms and increasing risk of disease. Changes temperature and precipitation in arctic, desert, alpine and boreal forest that could results into large change in species composition and biodiversity (Sala et al. 2000). A comprehensive study conducted by Poloczanska et al. (2013) to find the effect of warming ocean temperature concluded that the marine species are shifting poleward at a rate of 72 kilometers per decade which is faster than the terrestrial species.

1.3 Results

1.3.1 Trend analysis. We studied seasonal trends of precipitation and maximum and minimum temperatures for three different climatic zones of New Jersey for 110 years (1901-2010) (Table 4). The Northern part of the state shows the highest increasing trend of precipitation (0.635 mm/year) during the fall season with 95% confidence level. All three climatic regions exhibited greater increasing trend of precipitation during the fall season. Northern and Coastal regions manifest a small decreasing trend, -0.008 and -0.012 mm/year, for precipitation in the summer and winter respectively (Table 4), however, none of the trends were statistically significant. Also, our trend analysis suggested an increasing trend of precipitation in the Northern part compared with Southern and Coastal region (Table 4). In contrast to precipitation, there is strong evidence of increasing trend for both maximum and minimum temperature for all regions of New Jersey over all seasons at 99.9% confidence level. The Northern region exhibited highest increasing trend for maximum temperature (0.022°C/year) during winter

Table 4

Seasonal trend in precipitation (mm/year) and temperature (°C/year) for different climatic zones of New Jersey

Parameter	Season	Climatic zones		
		Northern	Southern	Coastal
Precipitation (mm/year)	Winter	0.243	0.122	-0.012
	Spring	0.443*	0.292	0.220
	Summer	0.167	-0.008	0.057
	Fall	0.635*	0.438++	0.475*
Maximum Temperature (°C/year)	Winter	0.022***	0.018***	0.018***
	Spring	0.015***	0.013***	0.014***
	Summer	0.013***	0.014***	0.015***
	Fall	0.014***	0.011***	0.013***
Minimum Temperature (°C/year)	Winter	0.020***	0.018***	0.021***
	Spring	0.013***	0.013***	0.017***
	Summer	0.018***	0.017***	0.020***
	Fall	0.015***	0.015***	0.018***

Note. *** Trend at $\alpha = 0.001$ level of significance; * Trend at $\alpha = 0.05$ level of significance; ++ Trend at $\alpha = 0.1$ level of significance. No sign means significance level > 0.1.

The highest increasing trend for minimum temperature was observed for Coastal region (0.021°C/year) (Table 4). Additionally, results indicate a greater warmer trend during winter season over the entire state of New Jersey.

1.3.2 Performance of bias correction. The relative performance of representing the annual cycle of precipitation and temperature simulated by the bias corrected GCMs and RCMs are highlighted in Figure 2.

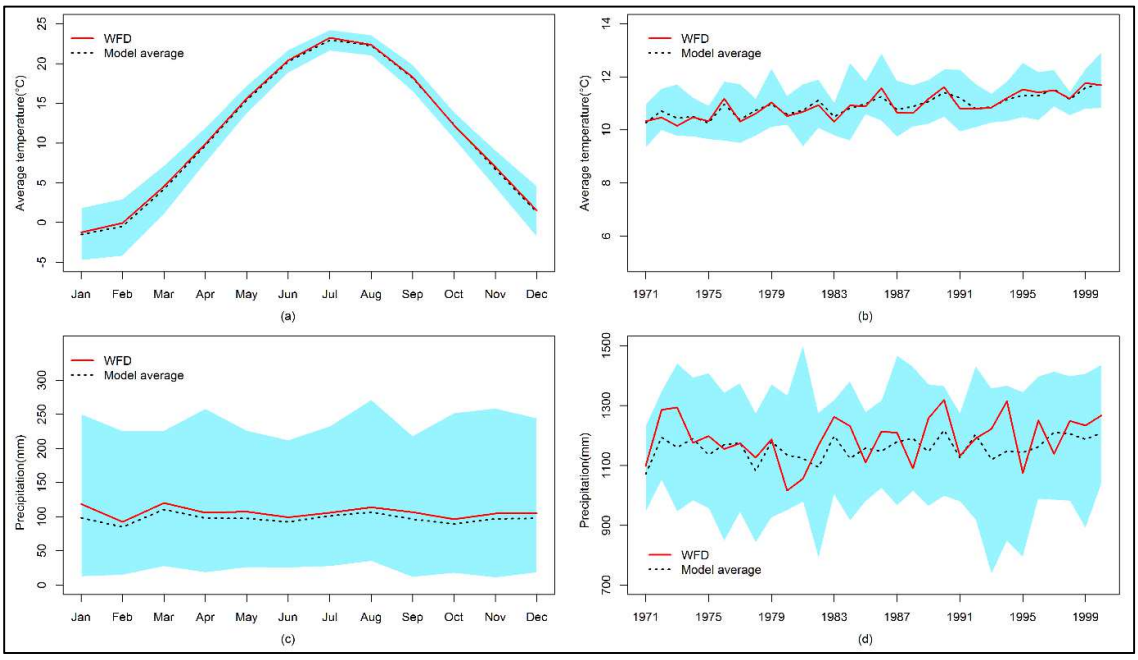

Figure 2. Comparison of annual cycle of average temperature and precipitation (a and c) and comparison of yearly average temperature and total precipitation (b and d) between observed WFD and bias corrected climate model dataset for 30-year period (1971-2000).

Both of the model simulated climatic parameter captured the annual cycle by comparison with the observed WFD dataset. The mean annual cycle of precipitation derived from the climate models slightly underrepresented the observed precipitation as shown in Figure 2c. Overall bias corrected climate models exhibit better representation of the annual cycle of temperature than the precipitation, indicating greater uncertainty still exists in climate

models. The yearly average of the 30-year period for both the observed and climate model data shown in Figure 2b and Fig 2d. Results indicated accurate representation of long term temperature pattern of the bias corrected climate models highlighted by the adjacency of the observed WFD with the mean of climate models derived average temperature (Figure 2b). The long term yearly precipitation pattern was also captured by the bias corrected GCMs and RCMs as shown in Figure 2d but with a greater level of uncertainty than the average yearly temperature.

1.3.3 Future temperature and precipitation projection. The average temperature anomaly for the 5 GCM and 5 RCM model is shown in Figure 3a relative to pre-industrial period (1861-1880) up to 21st century. As the greenhouse gas concentration increases sharp increasing trend was manifested for average temperature with the highest average temperature increase of 5.74°C in year 2092. Figure 3a suggests greater uncertainty in temperature projection as scenario extends to 21st century. Until 2040s both the ensemble mean of GCMs and RCMs projected similar temperature anomaly up to ~1.5°C over New Jersey considering the RCP 8.5 scenario. As the projection extends to near and far future the average temperature anomaly derived from the GCMs manifested greater increase than the ensemble mean of the RCMs as shown in Figure 3a. Considered individually, through the 21st century GCM MIROC exhibited the highest increase (~7.5°C) and the RCM GFDL-REGCM4 indicated lowest increase (~4.7°C). Unlike temperature the future projection of total precipitation up to 21st century exhibited lesser degree of increment over New Jersey with notable increase in the far future (2080s) as shown in Figure 3b. Ensemble mean of GCM precipitation predicts greater amount of total precipitation than the RCMs.

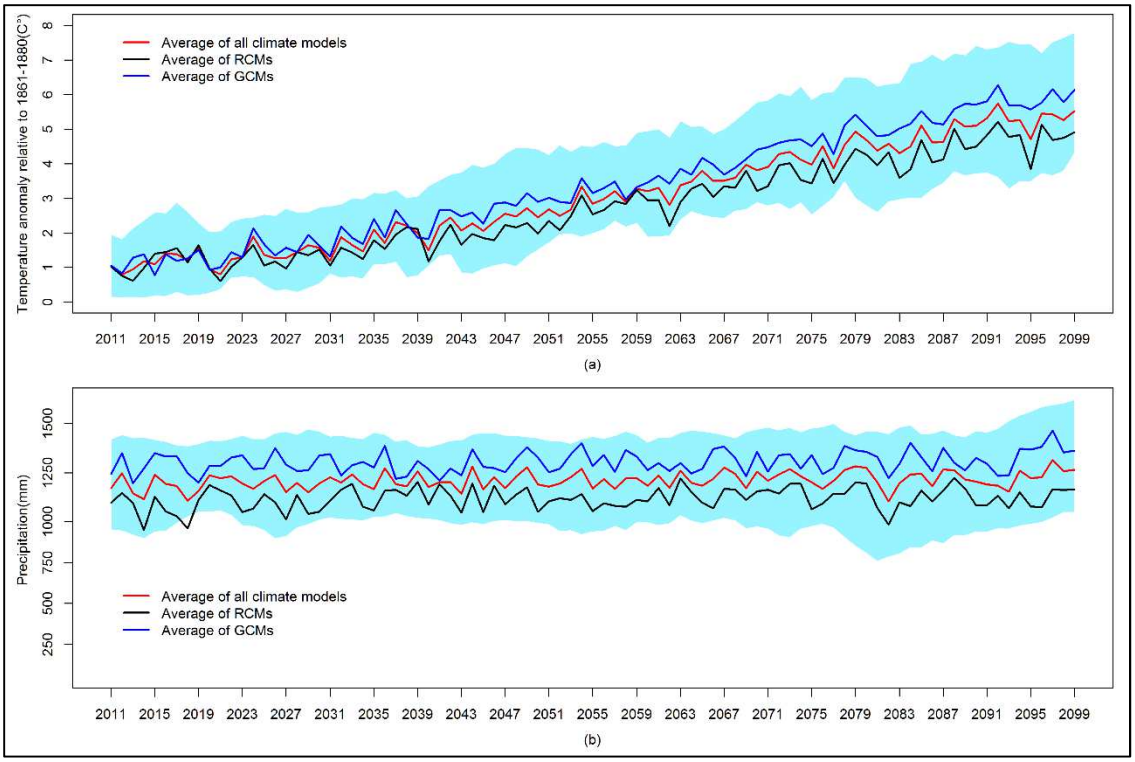

Figure 3. Temperature anomaly relative to 1861-1880 (a) and total precipitation (b) up to 21st century over New Jersey considering RCP 8.5 scenario.

1.3.4 Monthly variation of future average temperature and precipitation over New Jersey. Probable range of change in monthly variation of average temperature based on the climate models are represented in Figure 4. Results indicated highest increase in October during 2080s ranging between 3.8°C and 7.8°C over New Jersey. During 2020s and 2050s the annual cycle of temperature expected to increase up to ~2°C and ~3°C as shown in Figure 4. During 2080s the annual temperature cycle expected to surpass 6°C except for the month of March. Figure 4 also manifested greater temperature increase in late summer (August) as well as early and mid-fall (September and October) during 2080s. Results also indicated greater temperature increase during winter (December-January-February) than spring (March-April-May) for the three time periods. Future

changes of monthly precipitation under RCP 8.5 scenario for the GCMs and RCMs combined over New Jersey are shown in Figure 5.

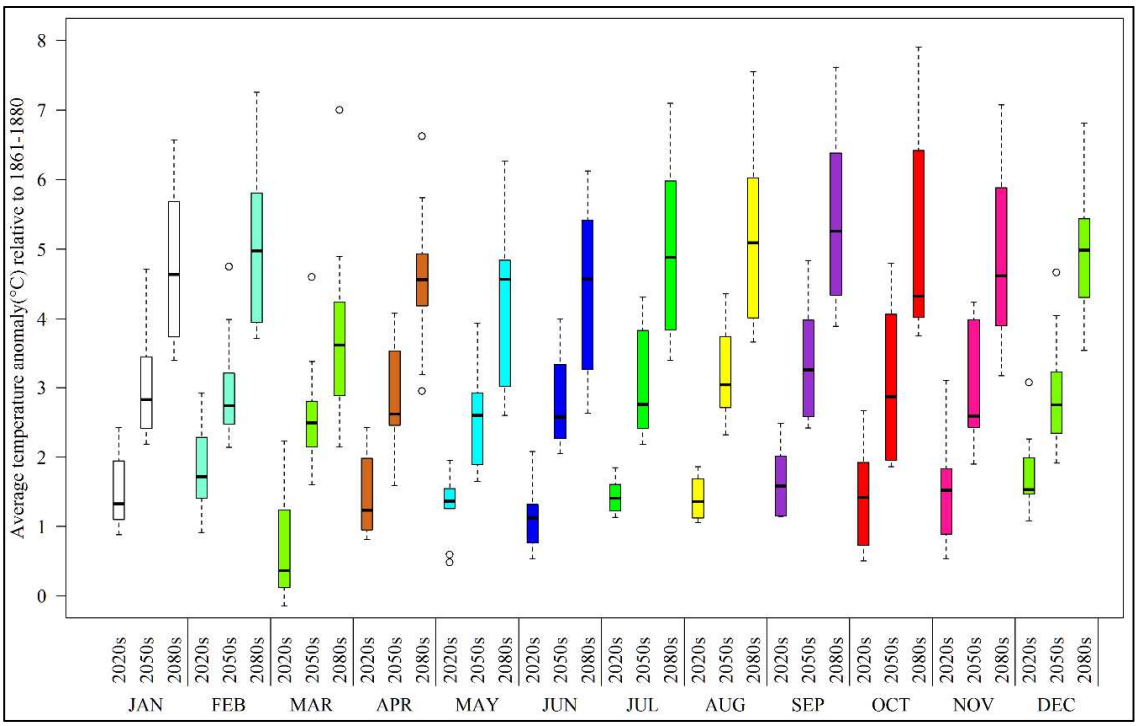

Figure 4. Monthly anomaly of average temperature relative to 1861-1880 for 2020s, 2050s and 2080s under RCP 8.5 scenario over New Jersey.

Results indicated that precipitation will increase in future in response to global warming under RCP 8.5 scenario. Model results suggested a significant increase of total monthly precipitation ranging between 55 mm – 150 mm up to 21st century during early and mid-winter (December and January) and early spring (March) than the other seasons. Least amount of precipitation increase was observed during October (~100) mm as shown in Figure 5.

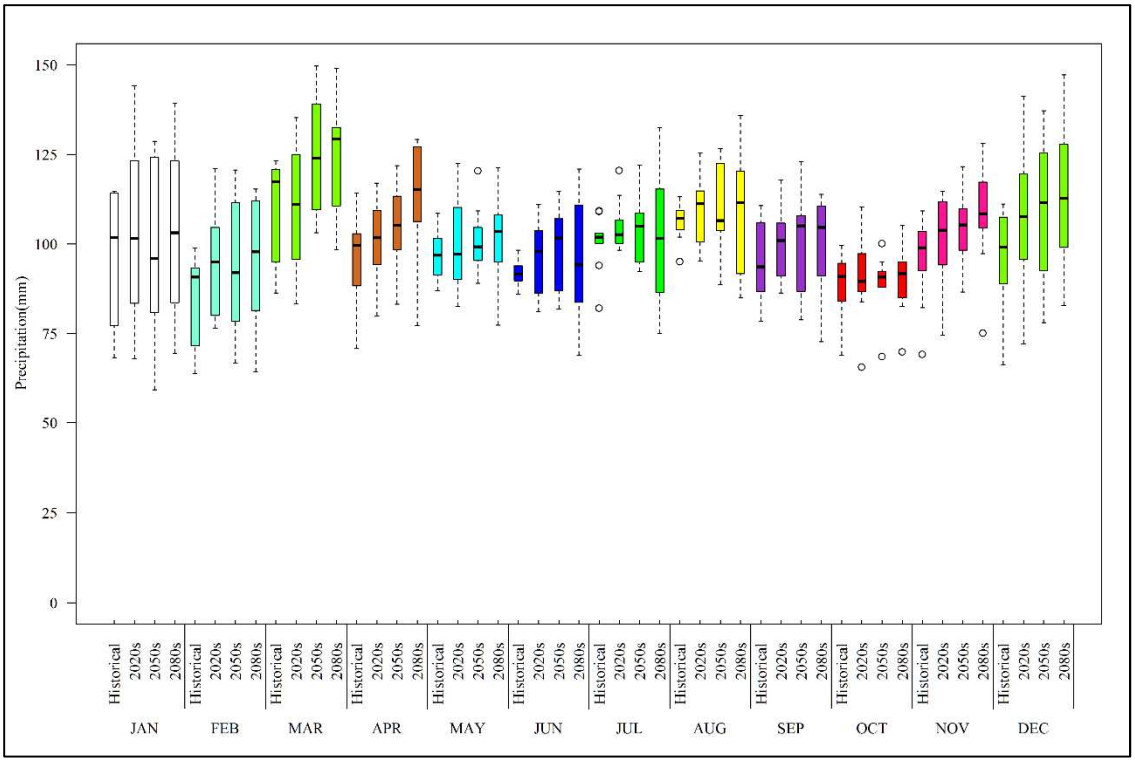

Figure 5. Projected future changes of monthly precipitation (mm) for 2020s, 2050s and 2080s with respect to baseline period of 1971-2000.

1.3.5 Spatial pattern of projected future changes of average temperature and precipitation over New Jersey. Projected spatial distributions of average temperature anomaly considering the RCP 8.5 scenario derived from the GCMs and RCMs over New Jersey for the three future time period (i.e. 2020s, 2050s and 2080s) are presented in Figure 6 and 7. All climate models resulted in a warmer temperature pattern over New Jersey, ranging between 1°C to ~5°C in comparison with the pre-industrial period. Both GCMs and RCMs exhibited up to ~2°C temperature increase over New Jersey during 2020s. Results also indicated that the GCM models predict greater temperature increment pattern than the RCM models. Results from the RCM models showed increasing temperature distribution up to ~3°C whereas the GCM models exhibited mixed

distribution ranging from 3°C to 4°C (GCM MIROC) even close to 4.5°C (GCM IPSL) during 2050s as shown in Figure 6 and 7.

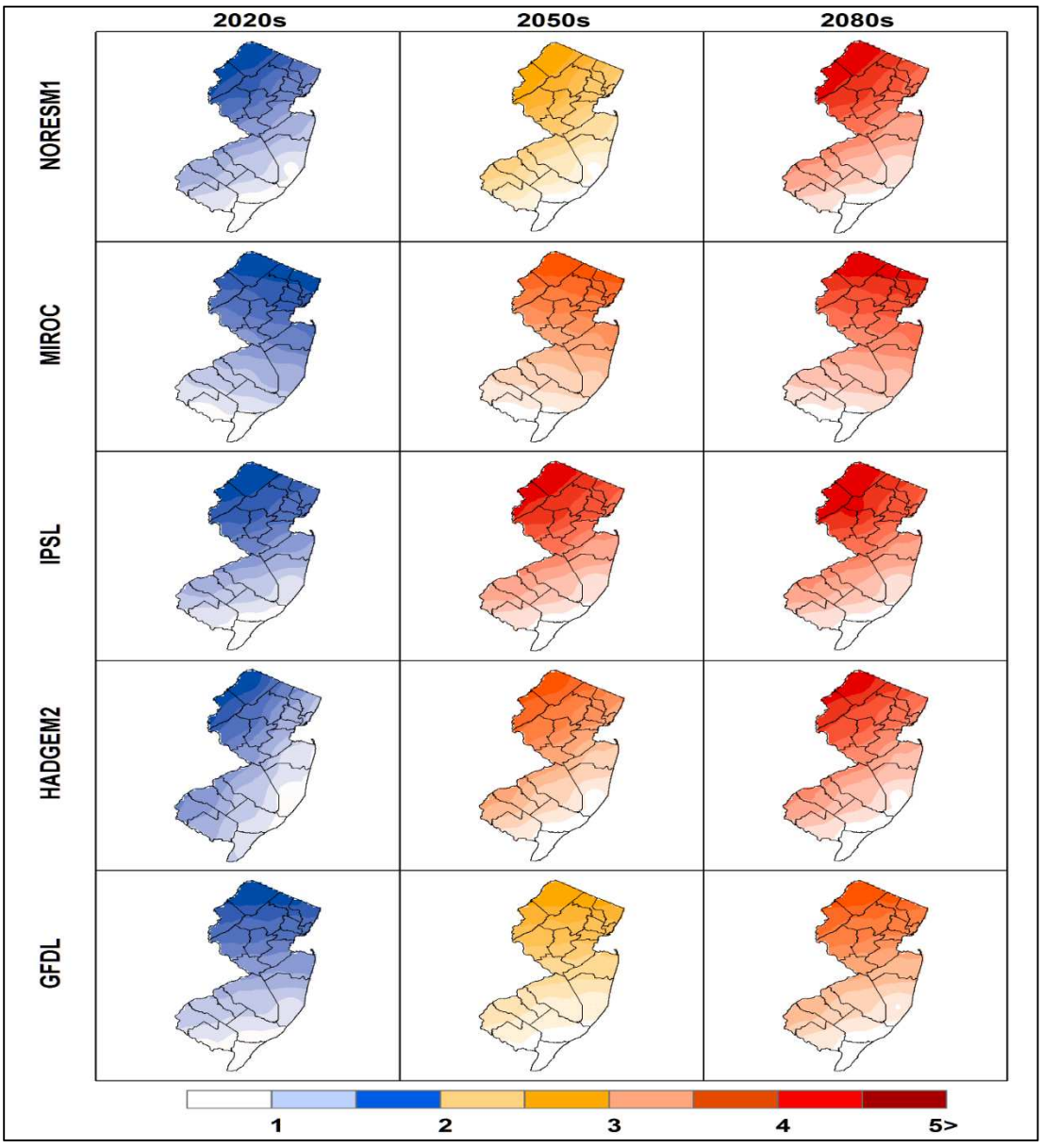

Figure 6. Spatial distribution of temperature anomaly (°C) relative to 1861-1880 over New Jersey derived from the GCMs for 2020s, 2050s and 2080s considering RCP 8.5 scenarios.

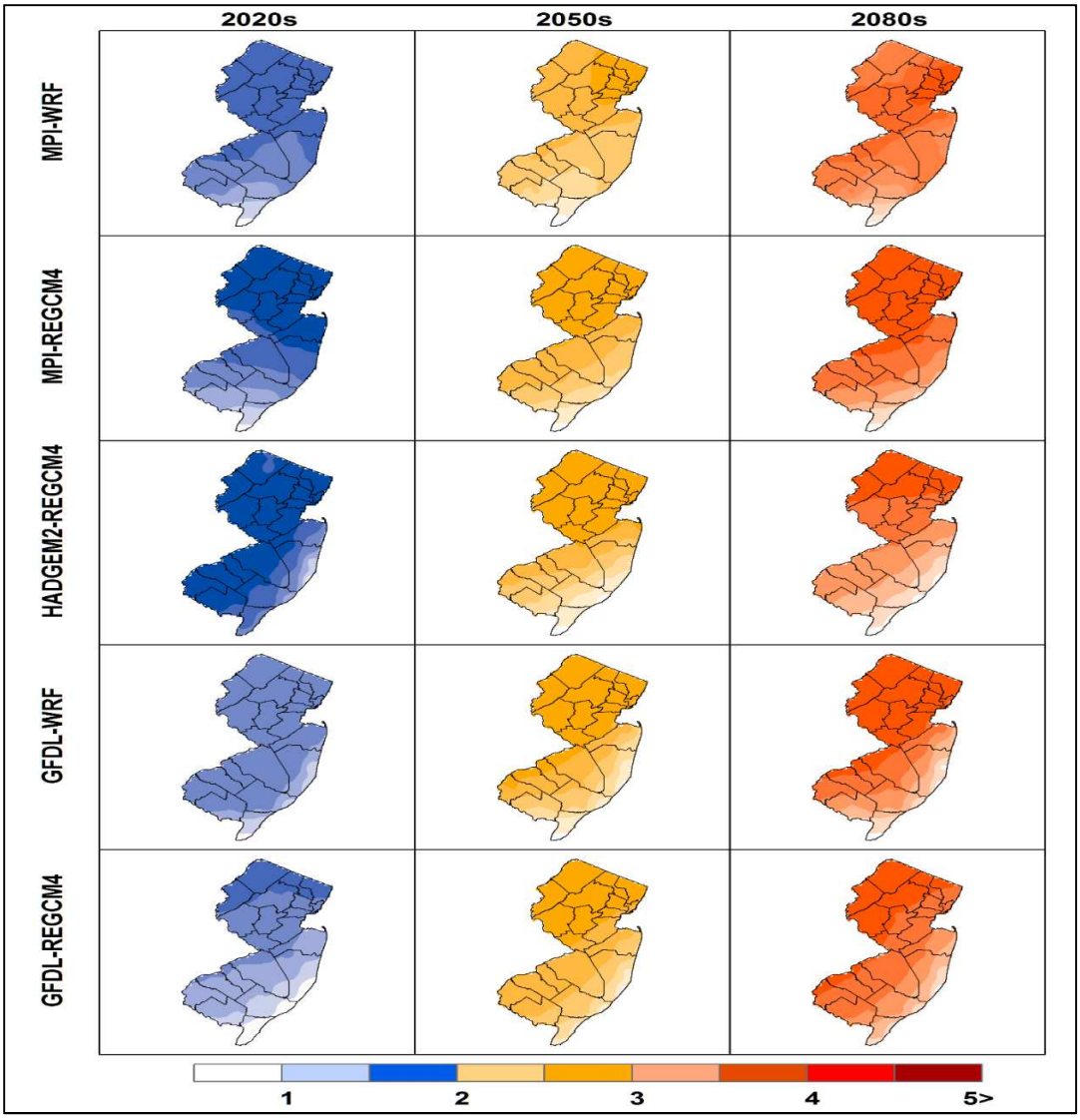

Figure 7. Spatial distribution of temperature anomaly (°C) relative to 1861-1880 over New Jersey derived from the RCMs for 2020s, 2050s and 2080s considering RCP 8.5 scenarios.

All the RCM models predicted a spatial increment of ~4°C whereas the GCM models exhibited greater than 4°C during 2080s except the GCM GFDL. A zonal distribution was evident from the spatial pattern of the models indicating greater increase of temperature in the Northern part of New Jersey. Counties like Sussex, Passaic, Bergen

and Warren which contain major business centers, are expected to face greater temperature rise.

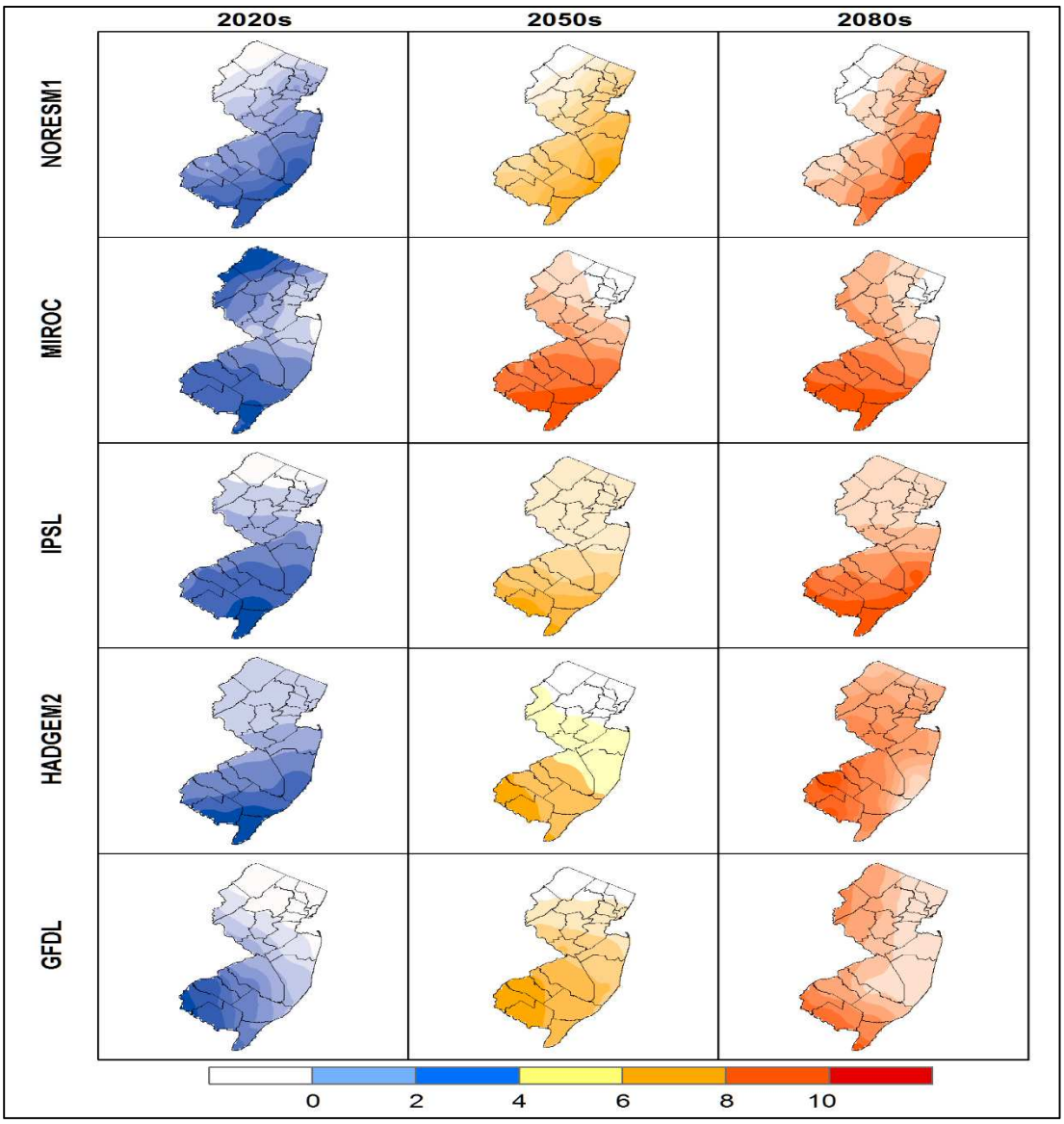

Figure 8. Percent (%) change of precipitation over New Jersey for 2020s, 2050s and 2080s derived from the GCMs considering RCP 8.5 scenarios relative to baseline period (1971-2000).

These urban areas are already facing issues with urban heat island effect. Temperature increase will likely worsen the situation causing serious health related issues. Spatial distribution of percent change of precipitation from the GCMs and RCMs considering the RCP 8.5 scenario over New Jersey for near, mid and far future are presented in Figure 8 and 9 respectively. The GCMs predicted an increase of total precipitation during 2020s with the highest percentage increase of ~4% in comparison to the historical period (1971-2000), especially on the Southern and South-East part of the New Jersey except GCM MIROC which projected significant increase in the Northern part of the state as well. All the GCM models showed an increase in total precipitation up to ~8% except GCM MIROC as shown in Figure 8. During 2080s part of Southern New Jersey is expected to receive increased precipitation (~10%) in comparison with the historical period (1971-2000) derived from the GCMs. The RCM models as shown in Figure 9 also showed an increase of total precipitation up to 4% except the MPI-REGCM4 and MPI-WRF which exhibited an early increase in total precipitation up to 8% during 2020s. During 2050s RCM model resulted in increase in total precipitation ranging between 2% to 10% except the RCM MPI-WRF which exhibited increase in total precipitation more than 10%. All the RCM models predicted an increase in total precipitation ranging between 6% to ~10 % during 2080s as shown in Figure 9. A zonal distribution is also highlighted by the climate models showing the Southern and South-Western counties such as Atlantic, Cape May, Cumberland, Salem and Camden of New Jersey are expected to be most vulnerable to increased precipitation in the future.

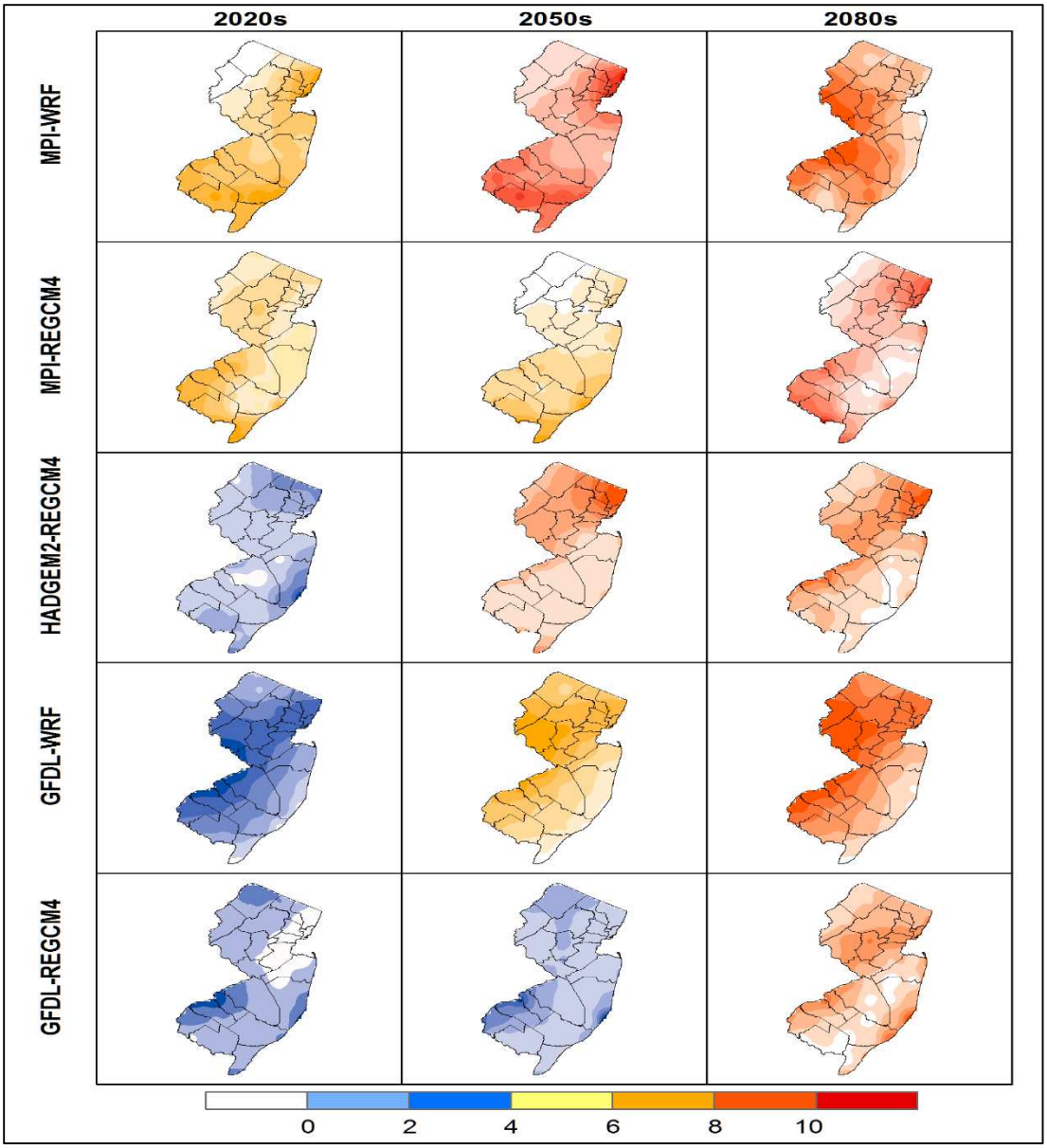

Figure 9. Percent (%) change of precipitation over New Jersey for 2020s, 2050s and 2080s derived from the RCMs considering RCP 8.5 scenarios relative to baseline period (1971-2000).

1.3.6 Extreme climate indicators. The temporal trend of the extreme climate indicators and their associated significance level are depicted in the Figure 10 and 11. The Consecutive Dry Days (CDD) and Consecutive Wet Days (CWD) are the indicators

of the length of the dry and wet season. All of the GCMs resulted in a statistically significant (p-value <0.05) increase in CDD with the highest trend exhibited by the GCM IPSL except the GCM MIROC which indicated a decreasing trend in CDD but it was not statistically significant (p-value > 0.05) as shown in Figure 10.

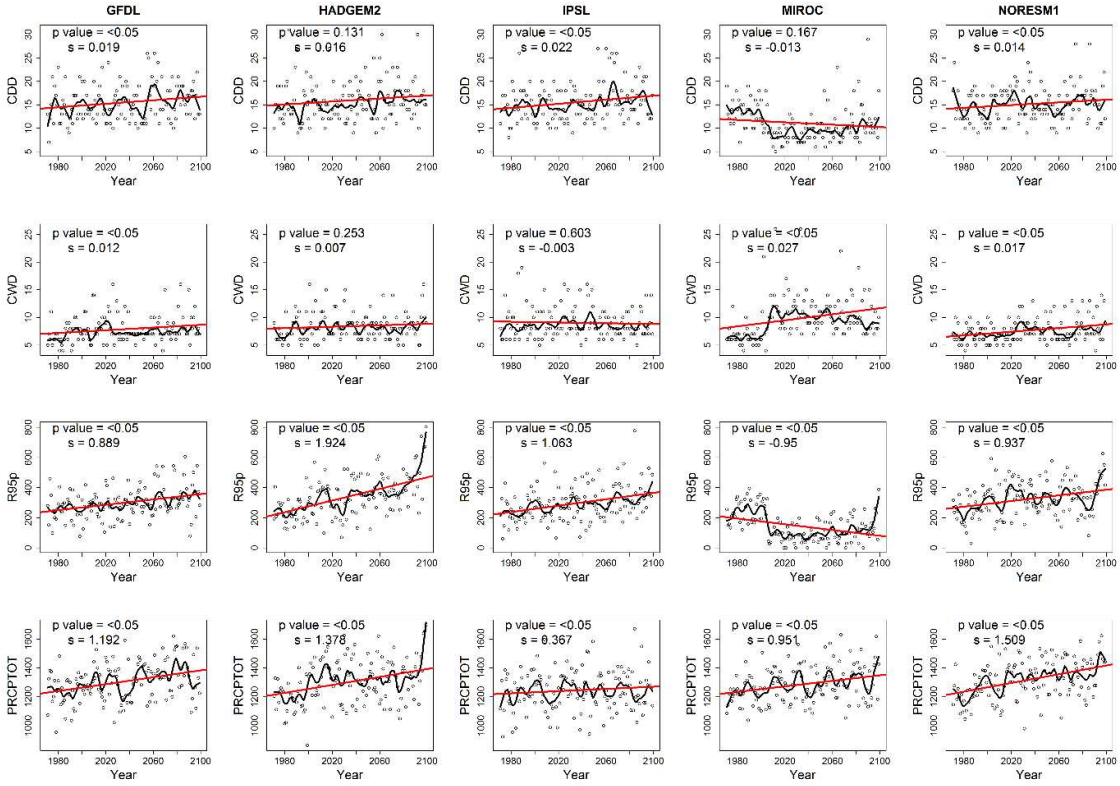

Figure 10. Extreme climate indicators as defined in Table 1.3 derived from the GCMs considering RCP 8.5 scenario over New Jersey

Similar statistically significant increasing trend was observed for the RCMs as well except the RCM MPI-WRF which indicated a decreasing trend in CDD but found to be not statistically significant as shown in Figure 11.

Statistically significant increase in CWD was also observed for the GCM GFDL, MIROC and NORESM1. Except that the both increasing and decreasing trend was manifested by the GCM HADGEM2 and IPSL respectively but none of them are statistically significant (p-value > 0.05) as shown in Figure 10. Apart from that, CWD derived from the only RCM MPI-WRF indicated statistically significant decrease in CWD.

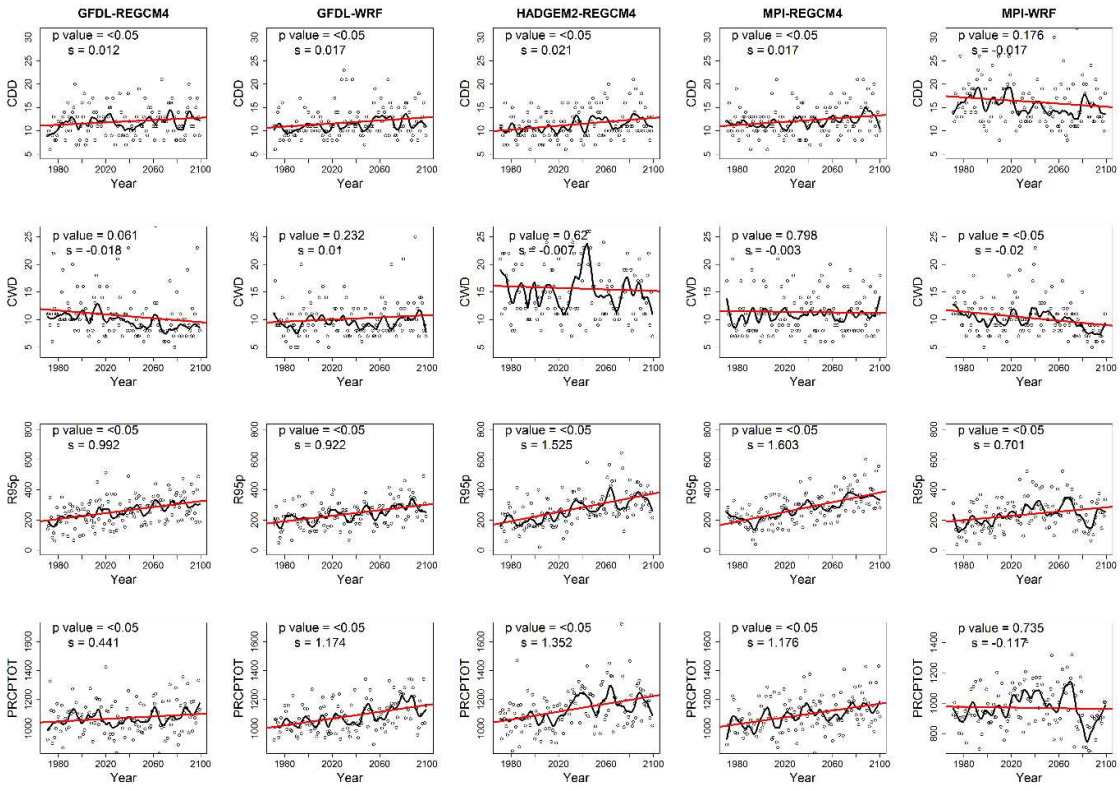

Figure 11. Extreme climate indicators as defined in Table 3 derived from the RCMs considering RCP 8.5 scenario over New Jersey

All of the climate models projected statistically significant increase in heavy precipitation (R95p) over New Jersey except for the GCM MIROC. The annual total wet-day precipitation index (PRCPTOT) derived from the climate models exhibited statistically significant increase in total precipitation in the future except RCM MPI-WRF which indicated a decreasing trend but found to be not statistically significant (p-value >0.05).

1.4 Discussion

Many studies, spanning several disciplines and employing different methods, have linked climate change to future temperature and precipitation patterns both in temporal and spatial scale. The increase of temperature in this study are in agreement with the results obtained by Karl et al. (1996) and Alexander et al. (2006). Hamlet et al. (2005) examined the increasing trend of temperature and its effect to the declining mountain snowpack in Western North America. Carlos et al. (2011) also analyzed the current trend of temperature and precipitation over Utah, USA and found similar increasing trend in temperature with few statistically significant trend in precipitation. It is a well-established fact that increasing air temperature will accelerate the water cycling process resulting in an increase in precipitation both in amount and intensity. Study conducted by Karl and Knight (1998) concluded 8% increase in precipitation across the United States since 1910. According to Kunkel et al. (1999) short duration extreme precipitation over United States is increasing at a rate of 3% per decade for the period of 1931-1996. A study conducted by Ahmed et al. (2013) over northeast United States using six GCMs and four RCMs also indicated similar trend in temperature and extreme precipitation. Implications of increasing temperature and precipitation over society and

ecosystems are studied in detail (Moberg and Jones 2005; Choi et al. 2009). Heat waves, floods and droughts, increasing frequency and intensity of hurricanes are direct consequence of changing climate. Agriculture is a key economic component generating $1.043 billion sales for the state of New Jersey. Changes in temperature and precipitation pattern will affect the growing season length, planting times, crop rotations, pest management and shifts in areas of crop production. According to several studies (Schlenker et al 2005; Ortiz et al. 2008) the projected temperature increase between 1.8°C and 5.4°C and precipitation extremes yields of major U.S crops and farm profits are expected to decline. Analysis also suggests that climate change has an influence on year to year swings in corn prices in United States (Diffenbaugh et al. 2012). Numerous hurricanes have passed near of through New Jersey in its history. Study conducted by Trenberth et al. (2005) indicated the changes in hurricanes intensity and rainfall due to warmer climate. New Jersey might face substantial economic loss due to stronger hurricanes. Tourism and outdoor recreation have been an important, growing sector of New Jersey's economy. Changes in precipitation and temperature patterns could have significant impacts on season lengths which in turn affect the economic viability of this industry.

1.5 Conclusions

This article presents an assessment of the expected future changes in the characteristics of precipitation and temperature over New Jersey considering the RCP 8.5 scenario using ten climate models. The current climatic trends of temperature and precipitation indicated temperature increase ranging from 0.13°C/decade to 0.2°C/decade for all regions of New Jersey with a high confidence level. Meanwhile, the current trends

for precipitation over New Jersey showed variations throughout the studied area and, in general, with few statistically significant trends. Thus, it was not possible to conclude that significant changes in precipitation occurred in this region over the last century. Bias corrected GCM and RCM outputs was found to represent the mean precipitation and temperature as well as small scale features of the annual cycle over New Jersey. It was also found that greater uncertainty still exist in the climate models in simulating precipitation compared to average temperature. By the end of the 21st century climate models projected an increase in temperature ranging from 3.5°C to ~7°C over New Jersey with greater temperature increase during winter season. Results indicated the Northern and Western part of New Jersey as the most vulnerable part under temperature increase. The winter precipitation expected to increase by 150 mm towards the 2080s relative to the baseline period of 1970s. The Southern and South-Western part of New Jersey will be most vulnerable to increase in total precipitation however, on smaller regional scale some regions may experience slightly lower rainfall in the future compared to the baseline period. Climate models exhibited strong evidence of increase in consecutive dry day (CDD) however prediction for consecutive wet day (CWD) do not agree under different climate models, suggesting uncertainty in the projection of precipitation changes. Increasing trend of CDD, R95p and PRCPTOT implies a longer drier season length with an increase of heavy precipitation in future. The scenarios presented in this article highlighted the expected changes in precipitation and temperature patterns over the coming years indicating future impacts of climate change over New Jersey. It is a high priority to detect these spatial and temporal changes in precipitation on the regional scales due to the associated critical socioeconomic consequences. Trends in regional

temperature and precipitation extremes and their indication of climate change are of interest to New Jersey as well as the rest of the world. Results obtained in the study corroborate the general idea that global warming is real and as a consequence increase in convective activity results in increase in total precipitation. Additionally, the data and methodology applied in this study can be extended to other regions as well. The main limitation of this study arises from the uncertainty in climate models to simulate the past and future climate. Inclusion of more bias corrected climate models to generate accurate multi model ensemble might improve the confidence of the results. Also, by including more than one emission scenarios could sufficiently capture the uncertainty in model predictions.

Chapter 2

Abstract

The eastern portion of New Jersey in the United States is vulnerable to flooding caused by hurricanes. A state of the art unstructured grid model known as Advanced CIRCulation (ADCIRC) was used to study the hydrodynamic response in the Western North Atlantic Domain (WNAT) during the superstorm Sandy of 2012, a notable example of hurricanes in this area. The model predictions were validated with the observed tide-surges and waves during this storm event. Waves and storm-tide circulation in the WANT domain were analyzed. The performance of ADCIRC model was evaluated by different statistical parameters to assess the model's ability to reproduce the storm-tide patterns. The overall root mean square error and Nash-Sutcliffe efficiency were in the order 0.2-0.5 m and 0.37-0.8, respectively. The shore of New Jersey plays an important role in dissipating the wave energy through the bottom friction when waves propagate from the ocean to the inner coast to its shallow bathymetry. The wind speed reached up to 45 m/s before Sandy made the landfall in Brigantine where the storm surge was 1.74 m as simulated by ADCIRC. Hurricane track files for different categories i.e. CAT1 to CAT5 were generated to simulate different scenarios. The wind speed increased from 45 m/s for CAT1 to 63 m/s for CAT5 hurricane. Highest water level for CAT5 hurricane was 3.56 m for Atlantic City.

2.1 Introduction

Coastal flooding along the Mid-Atlantic States is predominantly caused by the combination of elevated water levels and waves generated due to hurricanes as well as nor'easters (Schwartz 2007). A total of 294 North Atlantic Hurricanes has originated since 1851 producing hurricane force winds in 19 states along the Atlantic coast (Landsea and Franklin 2013) causing extensive damage to infrastructures as well as loss of lives. The challenge associated with the prediction of storm surges due to hurricanes arises from the nonlinear interaction between tides and storm surges (Dietrich et al. 2012). The generated waves also need to be resolved in accordance with the complex coastal bathymetry and configuration of coastline (Sebastian et al. 2014; Blain et al. 2008).

Numerical modeling plays an important role in understanding the hydrodynamics of water near the continental shelf. The simulated response from these hydrodynamic models largely depends on the computational domain, governing equations, boundary conditions, grid structure and forcing function itself. The models' performance in representing the hydrodynamic processes within shallow waters is based on understanding about numerical modelling. Numerous numerical models have been successfully implemented to simulate various oceanic behaviors such as tides, hurricanes, storm surges etc. (Sheng, 1987, 1990; Jelesnianski et al. 1992; Luettich et al. 1992; Hubbert and McInnes 1999; Casulli and Walters 2000; Sheng et al. 2006; Tang et al. 2014).

Normal tides, which have long wave periods, are generated by combined gravitational effects of the sun and moon on ocean waters (Schureman 1958, Melchior 1983). The basic characteristics of tide include wavelength, time period and amplitude.

These properties largely depend on the properties of a specific water body such as the bathymetry and coastal outline (Westerlink et al. 1992). Coastal areas are significantly influenced by the currents and water heights generated from tides, which significantly influence the overall coastal dynamics (Blain and Rogers 1998). The abnormal rise of water above the normal predicted astronomical tide during storm is known as storm surge whereas storm tide is the combination of total observed water level resulting from storm surge and the astronomical tide (NOAA 2017)

Basic mechanism for storm tide generation near the continental margin is comprised of several factors such as, astronomical tides originated due to relative positions of moon, sun and earth, pressure surge during hurricanes, wind driven surges and geostrophic tilt (Graber et al. 2006). Recent advancement in numerical simulation enables high spatial resolution in the field of hydrodynamic and wave modelling. Significant increase of accuracy in computed physics makes it possible to implement numerical modelling in coastal areas in order to assess their performance. As a result the combined mechanism of astronomical tides, storm surges due to wind and pressure, and wind induced waves during hurricanes have become well understood in recent years.

Superstorm Sandy also known as “Frankenstorm” is the second costliest tropical cyclone after Hurricane Katrina ever to strike the U.S (Blake 2013). The unprecedented track of Sandy with a sharp westward pushing across the New Jersey coast made the landfall with enormous size and powerful impacts spanning 24 states of U.S (Hall and Sobel 2013). Formed in Caribbean Sea it moved towards north and reached Category 3 hurricane at its peak. Hurricane Sandy was passing through the mid-Atlantic Bight when it took a sharp turn to the northwest on October 28, 2012 because of the favorable wind

flow pattern over Greenland and a mid-level trough coming from the U.S. southeast (Blake 2013, Hall and Sobel 2013). Hurricane Sandy made a landfall as a post-tropical cyclone on the New Jersey coast, striking densly populated urban areas including nearby New York City. On 29 October 2012, around 7:30 pm EDT (UTC-4), Hurricane Sandy made landfall near Brigantine, NJ, and resulted in an enormous impact on life and property damage, with the estimated cost exceeding $50 billion along the eastern seaboard (Force 2013, Mantell et. al 2013). The storm surge created some of the most devastating impacts, including flooding in New York City's subway tunnels, LaGuardia and Kennedy airports, damage to the New Jersey transit system, and the coastal seashore (NOAA 2012). When it made landfall, an abnormal storm tide with catastrophic, record-setting water levels occurred in New Jersey, New York City, and in a portion of Long Island Sound. The National Ocean Service (NOS) tide gages records show water level at The Battery, NY, Bergen Point, NY, Sandy Hook, NJ, Bridgeport, CT, New Haven, CT, at 2.74, 2.90, 2.44, 1.77, and 1.69 meters above mean higher high water, respectively (NOAA 2012). The worst flooding occurred over Staten Island and to the south along the New Jersey shore. The storm surge also caused significant flooding in parts of the Hudson River Valley, the East River, and the western part of Long Island Sound.

Storm surges generated during extreme storm events cause substantial damage to coastal communities, and therefore, it is very important to understand the formulation of storm tides through numerical modeling for better preparation in future. The work described in this study focuses on numerical modelling of normal tidal circulation and storm tides in coastal waters. Particularly, sensitivities of the tidal circulation, storm tides elevation and historical hurricane scenarios simulated using ADCIRC-2DDI model are

investigated. Additional considerations during numerical modelling such as ocean boundary conditions, nonlinear properties of tidal dynamics and optimum grid resolution are also described.

2.2 Domain and Model Formulation

2.2.1 The Western North Atlantic Tidal (WNAT) model domain. The current trend in coastal ocean tidal modelling by utilizing larger computational domains has been demonstrated by previous research (Westerink et al. 1994, 1995).

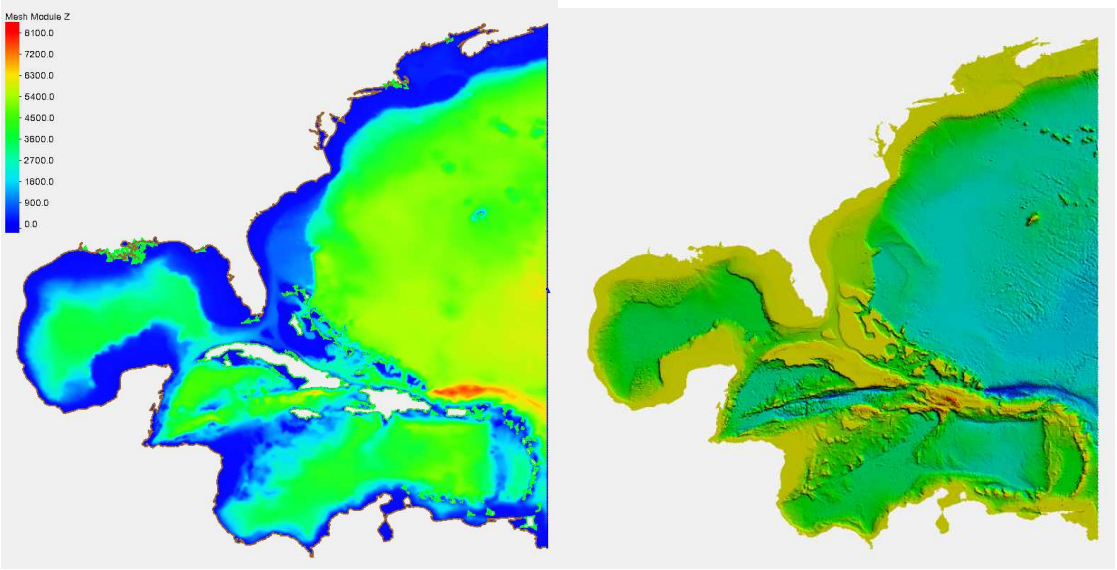

Figure 12. WANT model domain and ocean bathymetry.

Study conducted by Flather (1988), Vincent and Le Provost (1988), Hagen and Parrish (2004) and recently Cialone et al. (2017), Bacopoulos and hagen (2017) have all implemented tidal and/or storm surge models considering a large portion of the North

Atlantic region. These studies concluded that precise tidal predictions can be simulated using large computational domains through hydrodynamic modelling. The advantage of using a coastal models with large computational domains allow accurate specification of boundary conditions, because the open boundaries are placed in the deep ocean where flow behavior is linear, and tidal constituents may be more accurately defined. The open ocean boundary of the WNAT model encloses the Western North Atlantic Ocean, the Gulf of Mexico and the Caribbean Sea (Figure 12). The open ocean boundary for the WNAT model domain lies along the 60°W meridian extending from the area of Glace Bay, Nova Scotia, Canada to the vicinity of Corocora Island in eastern Venezuela and is situated entirely in the deep ocean (Figure 12). This large computational domain covers an area of approximately 8.4 million km^2. Because of its great size and since high resolution was required in coastal regions to adequately represent geometry and tidal flow, we applied to the present model application an unstructured mesh so that we may provide high resolution in areas of shallow water, steep bathymetry and rapidly changing bathymetric gradient, while providing lower, though still adequate, resolution in the deep ocean. The grid consists of approximately 53,000 nodes (Figure 13). The topography within WANT domain includes the continental shelf with a depth varying from 0 m to 130 m and the continental rise and deep ocean (depths from approximately 3000 m to almost 8300 m) as shown in Figure 13.

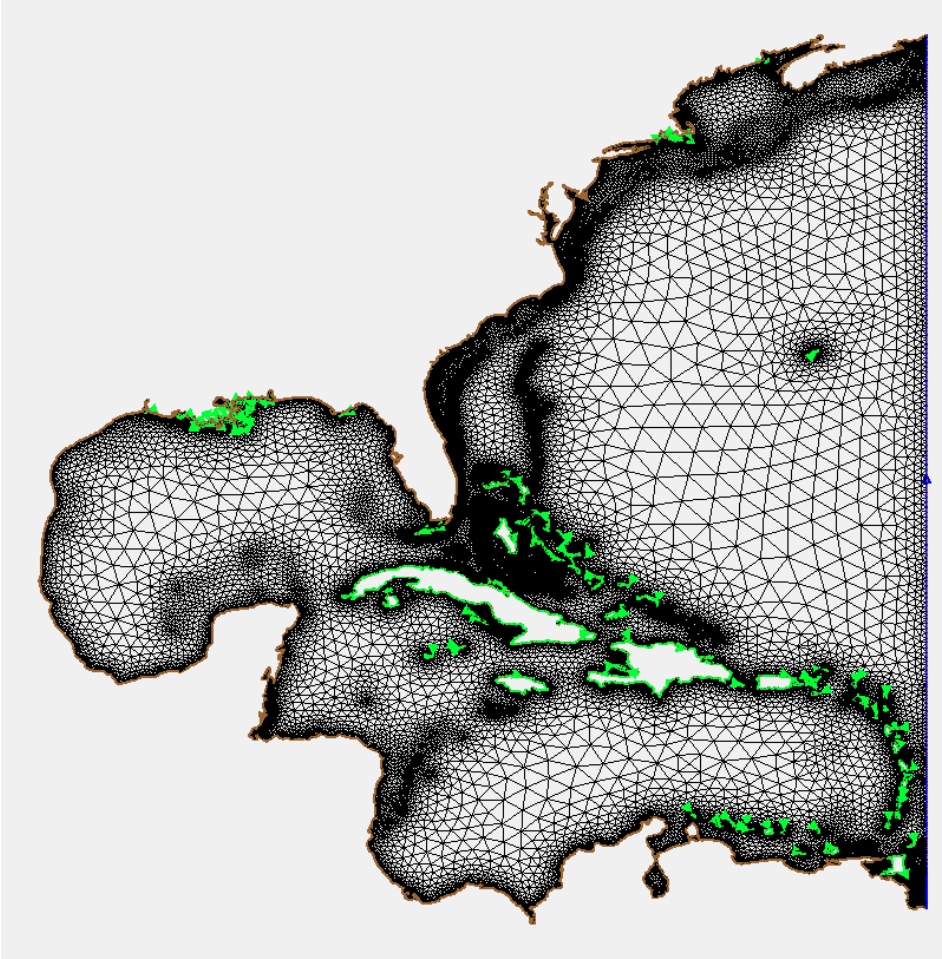

Figure 13. Unstructured mesh in WANT model domain.

2.2.2 Shoreline, ocean bathymetry data and observation data. The required seashore boundaries were defined by the Global Self-consistent, Hierarchical, High-resolution Geography Database (GSHHG) (Wessel and Walter 1996). This high resolution shoreline dataset amalgamated from two databases in the public domain: World Vector Shorelines (WVS) and CIA World Data Bank II (WDBII).

Figure 14. Locations of observed data from NOAA.

The data was obtained from the National Centers for Environmental Information (NCEI) in ESRI shapefile format with WGS84 geographic horizontal datum (source: https://www.ngdc.noaa.gov/mgg/shorelines/). Bathymetry data from National Geophysical Data Center (NGDC) was available for the whole WNAT study region. The ETOPO1 1 arc-minute bathymetric dataset is a global relief model of earth's surface that integrates land topography and ocean bathymetry (Amante and Eakins 2009). ETOPO1 is vertically referenced to sea level, and horizontally referenced to the World Geodetic System of 1984 (WGS 84). Cell size for ETOPO1 is 1 arc-minute (~2.5 km). NOAA's VDATUM (parker et al. 2003) was used to convert the bathymetry data to the common vertical datum NAVD88. Hourly observed water level data from NOAA was collected

from 21st October to 1st November, 2012 for 13 stations as shown in Figure 14 were used to validate the results from ADCIRC simulation.

2.2.3 ADCIRC model. The ADCIRC model, developed by Luettich et al. (1992) and Westerlink et al. (1994), was used to simulate the response of water levels and currents to the superstorm Sandy in the WANT model domain. The two-dimensional (2D) depth-integrated version, often referred to as ADCIRC-2DDI, was used in this study. It basically solves generalized wave continuity equations on an unstructured triangular mesh with a continuous Galerkin finite element method (Van and Van 2002). By using an unstructured triangular mesh, the model is capable of resolving complex geometry and bathymetry. The governing equations in spherical coordinate system are as follows:

$$\frac{\partial \zeta}{\partial t} + \frac{1}{R\cos\phi}\left[\frac{\partial (UH)}{\partial \lambda} + \frac{\partial (VH\cos\phi)}{\partial \phi}\right] = 0 \tag{2.1}$$

$$\frac{\partial U}{\partial t} + \frac{1}{R\cos\phi} U\frac{\partial U}{\partial \lambda} + \frac{V}{R}\frac{\partial U}{\partial \phi} - \left(\frac{\tan\phi}{R} U + f\right) V = -\frac{1}{R\cos\phi}\frac{\partial}{\partial \lambda}\left[\frac{P_s}{\rho_0} + g(\zeta - \alpha\eta)\right] + \frac{\upsilon_T}{H}\frac{\partial}{\partial \lambda}\left[\frac{\partial (UH)}{\partial \lambda} + \frac{\partial (VH)}{\partial \phi}\right] + \frac{\tau_{s\lambda}}{\rho_0 H} - \tau * U \tag{2.2}$$

$$\frac{\partial V}{\partial t} + \frac{1}{R\cos\phi} U\frac{\partial V}{\partial \lambda} + \frac{V}{R}\frac{\partial V}{\partial \phi} - \left(\frac{\tan\phi}{R} U + f\right) U = -\frac{1}{R}\frac{\partial}{\partial \phi}\left[\frac{P_s}{\rho_0} + g(\zeta - \alpha\eta)\right] + \frac{\upsilon_T}{H}\frac{\partial}{\partial \phi}\left[\frac{\partial (VH)}{\partial \lambda} + \frac{\partial (VH)}{\partial \phi}\right] + \frac{\tau_{s\phi}}{\rho_0 H} - \tau * V \tag{2.3}$$

Where t is time; λ and ϕ are longitude and latitude, respectively; ζ is the free surface elevation relative to geoid; U and V are depth-integrated velocity component in west-east and south-north directions, respectively; $H = \zeta + h$ is the total water depth and h is the bathymetric water depth relative to the geoid; f is the Coriolis parameter, where

Ω represents the angular speed of the earth, and, $f = 2\Omega Sin$; P_s is the atmospheric pressure at the free surface; η is the Newtonian equilibrium tide potential; α is the effective earth elasticity factor; ρ_0 is the reference density of water; R is the radius of the earth; g is gravitational acceleration; $\tau_{s\lambda}$ and τ_s are the surface wind stress in longitudinal and latitudinal directions, respectively, which are computed by a standard quadratic air sea drag law, and the air sea drag coefficient is defined by Garratt's formula (Garratt, 1977); $\tau*$ is defined as

$$\tau = \frac{C_f \left(U^2 + V^2\right)^{1/2}}{H} \tag{2.4}$$

Where C_f is the bottom friction coefficient

2.2.4 Model parameters. The ADCIRC-2DDI model was used to simulate storm surge. The finite amplitude and convection terms were activated. Lateral viscosity was set at a constant of 4 m^2/s through the whole domain (Hench and Luettich 2002; Yang and Myers 2008). The varying bottom friction depending on shallow or deep water was specified using a hybrid bottom friction relationship (Luettich and Westerlink 2006):

$$C_f = C_{fmin}\left[1 + \left(\frac{H_{break}}{H}\right)^{\theta_f}\right]^{\frac{\gamma_f}{\theta_f}} \tag{2.5}$$

where C_{fmin} is the minimum bottom friction coefficient, H_{break} is the break depth, θ_f is a dimensionless parameter that determines how rapidly bottom friction relationship

approaches its deep water or shallow water limits when the water depth is greater than or less than H_{break}, and γ_f is a dimensionless parameter that determines how the friction factor increases as the water depth decreases. When the water depth is less than H_{break}, the formulation applies a depth-dependent, Manning-type friction law, while a standard Chezy friction law is used when the depth is greater than H_{break}. The parameters were set to C_{fmin} =0.03, H_{break}=2.0m, θ_f =10 and γ_f =1.3333 as recommended by Luettich and Westerlink (2006).

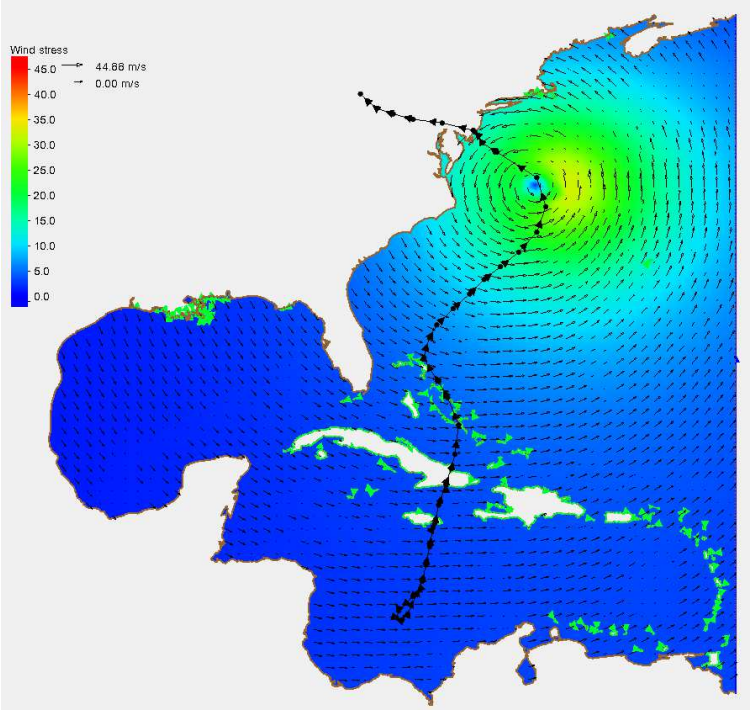

Figure 15. Track of hurricane SANDY in ADCIRC model.

The eight most important tidal constituents (M2, S2, N2, K2, K1, P1, O1, and Q1) were used as a tidal forcing along the open ocean boundary. The time step for the ADCIRC model was set to 5.0 second to achieve computational stability. The required hurricane SANDY best track file was obtained from http://tropicalatlantic.com. The best track file was obtained in ATCF format which has the information about as shown in Figure 15 provides the required data for atmospheric pressure, coordinates of the hurricane tracks as well as timing. The duration of ADCIRC simulation was from 21st October 2012 to 31st October 2012. Sandy was a superstorm when it made the landfall. To assess the impact of different categories of hurricane it was required to create hurricane track files for different hurricane categories (i.e. CAT to CAT5). The required information such as hurricane direction was kept the same and thus the location of landfall, but the wind velocity, radius and atmospheric pressure during different categories of hurricane were obtained from hurricane Katrina because Katrina went through all phases of hurricane categories along its way to landfall. This synthetically generated hurricane track files were then imported to ADCIRC model as an input for wind parameter.

2.3 Results and Discussion

Model validation was performed to ensure that ADCIRC adequately predicts the hydrodynamics of the study area. The model accuracy is influenced by the accuracy of the forcing functions applied in the open ocean boundaries, accurate representation of the geometry of the study area (i.e. coastline and coastal bathymetry) and values selected for model parameter such as wave continuity, bottom stress etc. A satisfactory agreement between predictions and measurements in the validation procedure ensures confidence

that modelling represents the pertinent hydrodynamic process. The results for the model validation in this study was accomplished by comparing the observed data with ADCIRC simulated data for 13 tidal stations from NOAA

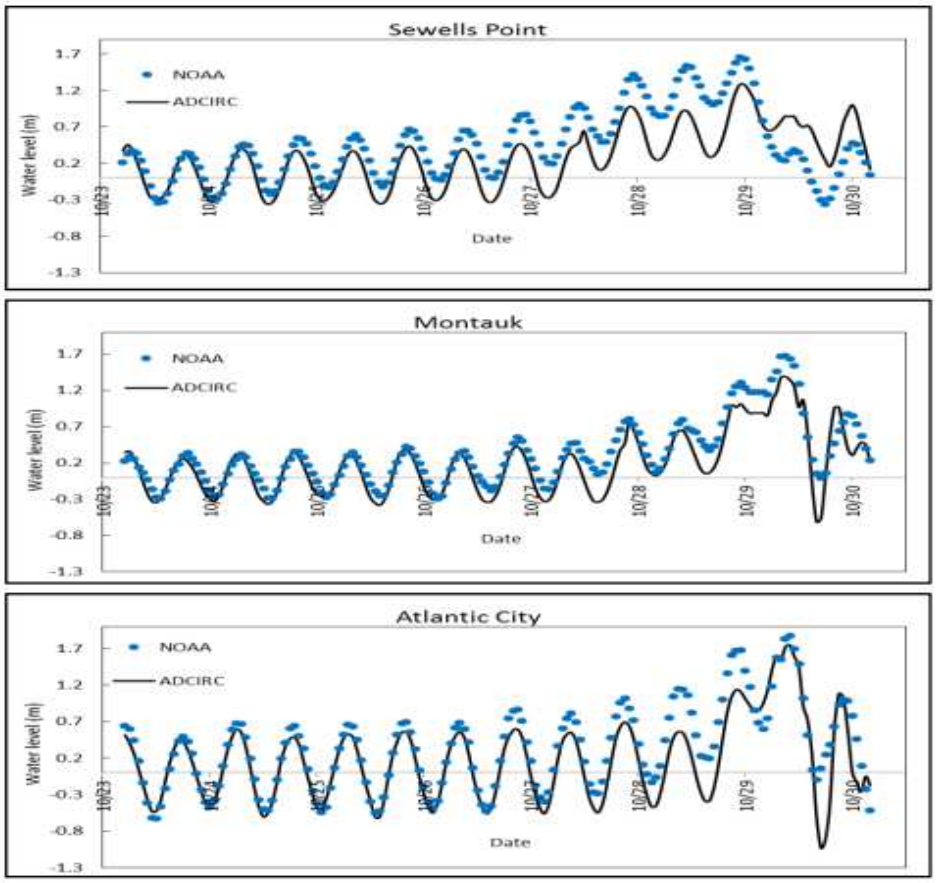

Figure 16. Example comparison of water level (m) from ADCIRC simulation with the observed data

To quantify the accuracy of the observed and model simulated data, different statistical parameters such as Nash-Sutcliffe efficiency (NSE), Root mean squared error (RMSE), Mean absolute error (MAE), Coefficient of determination (R-square), Pearson

correlation coefficient, Ratio of standard deviations were used. Figure 16 exhibits the performance of ADCIRC simulation in comparison with the observed water level data. ADCIRC simulation was able to represent the observed tidal pattern.

Table 5

Statistical parameters to compare observed and ADCIRC simulation results

	NSE	RMSE	MAE	RSquare	Pearson correlation	Ratio of Standard Deviations
Montauk	0.779	0.207	0.162	0.873	0.934	0.955
Kings Point	0.776	0.491	0.357	0.866	0.931	1.034
Sandy Hook	0.727	0.359	0.273	0.851	0.923	0.925
Atlantic City	0.743	0.290	0.206	0.833	0.913	0.958
Cape May	0.610	0.389	0.274	0.796	0.892	0.901
Ship John Shoal	0.370	0.516	0.391	0.706	0.840	1.032
Brandywine Shoal Light	0.779	0.274	0.193	0.795	0.891	0.856
Lewes	0.542	0.396	0.272	0.742	0.861	0.852
Ocean City Inlet	0.745	0.213	0.157	0.769	0.877	0.879
Wachapreague	0.747	0.266	0.203	0.784	0.885	0.946
Kiptopeke	0.510	0.302	0.227	0.626	0.792	0.899
Sewells Point	0.416	0.371	0.318	0.565	0.751	0.832
Chesapeake	0.805	0.212	0.179	0.919	0.959	0.953

The simulated normal tide was found to be slightly lower than that of observed data in high tide, which could be due to overestimation of bottom friction in the ADCIRC model. The peak water level during Sandy was also well captured by the ADCIRC model. Results shown good agreement between the observed peak and decay of water level in Atlantic City station near which Sandy made the landfall. The Rsquare represents the combined dispersion against the single dispersion of the observed and model simulated results. Therefore the systematic over and underrepresentation of observed tidal surge simulated by ADCIRC could be overlook.

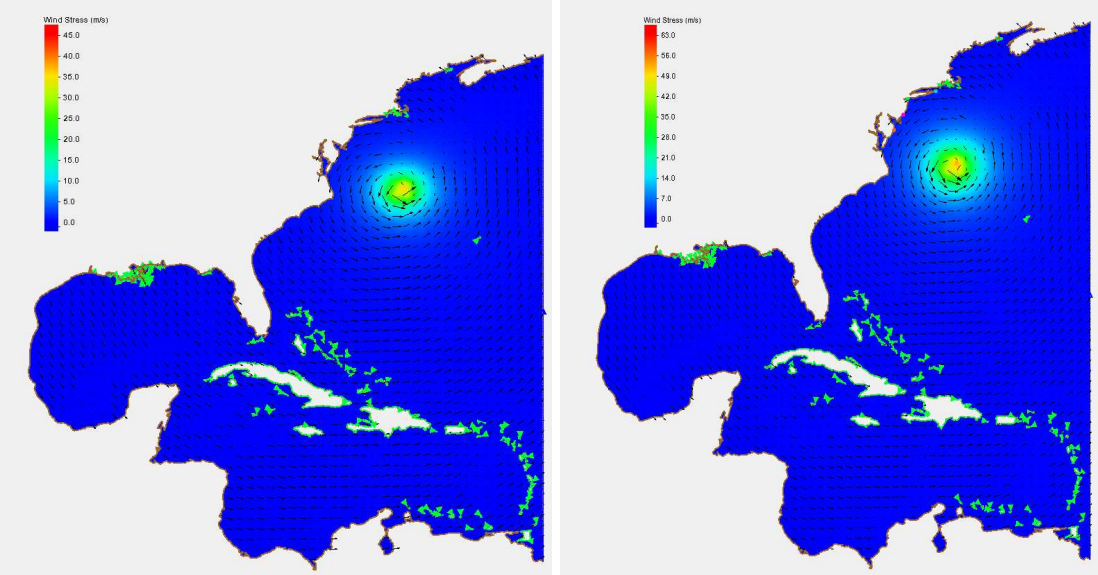

Figure 17. Wind stress for CAT1 and CAT5 hurricanes near the coast of New Jersey

Thus, NSE was used which is not very sensitive to systematic model over or under prediction especially during low flow periods. The Nash-Sutcliffe model efficiency

coefficient as shown Table 5 exhibits that except Cape may, Lewes and Ship John Shoal all the other stations performed very well to capture the peak storm surge generated by ADCIRC (NSE <0.7). More refined mesh and better bathymetric data near the shoreline could have solve the issue for those three stations mentioned above. Although the Rsquare and Pearson correlation manifested that ADCIRC model simulated water level accurately represents the tidal pattern, peak and rise of the observed stations during the period of simulation concluding a better fit between observed and model. The ratio standard deviations also suggest that the variability of the observed were well represented by the ADCIRC model as they are close to 1. Once the ADCIRC model was validated to represent the observed storm-tide, the synthetic wind files generated before were used to simulate different categories of hurricane scenarios.

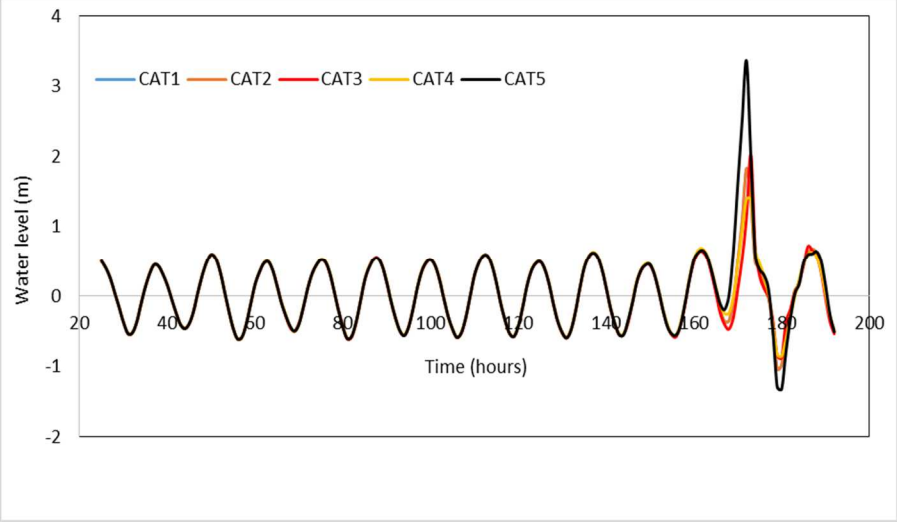

Figure 18. Water level at Atlantic City station for different categories of hurricane simulated from ADCIRC

Figure 17 represents the wind stress or wind velocity comparison between a CAT1 hurricanes to CAT5 hurricane categories. Results exhibited increase of wind velocity from 45m/s for CAT1 to 63m/s for CAT5 from ADCIRC simulation. Related water level for different categories of hurricanes for Atlantic City station from ADCIRC simulation were depicted in Figure 18. As the intensity of hurricane increases water level also rises from CAT1 to CAT5 hurricanes. The highest water level was observed as 3.56 m for CAT 5 hurricane.

2.4 Conclusion

In October of 2012, an intense nor'easter, superstorm Sandy, swept through the east coast of New Jersey and caused significant coastal flooding and severe beach erosion along the north Atlantic coastline. A state-of-the-art model ADCIRC model was used to study the hydrodynamic response to this notable storm in the Western North Atlantic Domain. The model reasonably reproduced the tides and storm surges and large waves compared with tide gauge. Wave distribution and circulation were analyzed and the following can be concluded:

(1) The resolution of the coastal bathymetry and shoreline is an important factor to represent the actual near coast characteristics through ADCIRC modelling.

(2) High resolution unstructured grid, which greatly impacts the hydraulics of tidal storm surge, is essential for capturing the actual storm scenarios. Although, increasing the number of mesh near the shoreline cloud increase the accuracy of the model results, but it also required extensive computational capacity. If computational resources are available, simulations with finer grid and additional storm scenarios could provide effective tools

for flood prevention structures near coast and assessment of potential storm surge impact on coast of New Jersey.

(3) The water level vs time data obtained for different categories of hurricane could be an important resource to understand the probable range of storm surge. This data could also be the input boundary condition for inland flood modelling.

(4) The system developed through this research could provide valuable information for nearshore marine operations by predicting hurricane storm surge and flooding.

(5) Long term simulation of tides and wind driven water circulation could model the impact of potential sea level rise on coastal communities.

Chapter 3

Abstract

Developing an effective real-time evacuation strategy during extreme storm events such as hurricanes have been a topic of critical significance to the emergency planners and response community. The spatial and temporal variability of inland flooding during hurricanes present more challenges for a robust evacuation planning. In this study a framework was developed to combine results from hydrodynamic modelling and traffic simulation for real time evacuation planning. First a dynamic 2D hydrodynamic model was developed to provide information about flood depth and velocity for the evacuation routes during storm event. Traffic microsimulation was conducted using the information from hydrodynamic model which provides the information about traffic velocity on the evacuation routes during the event. The last component of the framework includes combining results from both models to develop GIS files. Results from this framework could be easily access by general public and decision makers for efficient evacuation planning during extreme storm events.

Keywords: Evacuation, Hurricanes, Flood modelling, Traffic Simulation, Framework

3.1 Introduction

Natural disasters can strike anywhere at any time, often without warning. The spatial and temporal variability of these extreme events create complex location specific problems that require real-time or near real-time decision making support. A robust decision making support framework can develop resilient communities by providing on-time decision support such as potential threats to the critical structures, evacuation

strategies, and dissemination of critical information to users of the community. This study focuses on integrating hydrodynamic modelling with traffic micro simulation to provide better decision support for evacuation planning during hurricanes. There are two primary components of the decision making support framework; (1) hydro dynamic modelling for flood scenarios, that provides an estimate of in-land flooding before, and during the hurricane land fall; (2) a traffic micro-simulation model for the Brick township, NJ that provides critical evacuation routes and movement of users during evacuation.

Flooding during extreme storm events are natural hydrological event which is becoming more frequent due to global warming and sea level rise (Hallgatte et al. 2013; Hirabayashi et al. 2013; Tebaldi et al. 2012). Flood hazard during any storm event is assessed by simulating the physical processes through numerical modelling of the flood using boundary conditions and predicting the potential flood extent, depth and velocity inland (Hartanto et al. 2011; Beevers et al. 2012; Ballica et al. 2012). There are several numerical tools currently available for flood propagation and inundation modelling. The physics behind these models are based on the mathematical conservation laws for mass and momentum. For example Pender (2006) classified hydraulic models considering to the dimensionality of the solution algorithm as shown in Table 6. Uncertainty in flood modeling arises from coarse topographic detail, solution algorithm as well as from modelling assumptions. For example Bates et al. (2009) concluded that the assumption of fixed channel geometry for inundation modelling may not represent geomorphic change in river geometry during very large floods. Also, water exchange with the surrounding catchment is not under consideration for many numerical models of floodplain flow.

Table 6

Summary of numerical tools for flood modelling and their potential application (Pender 2006)

Method	Description	Software examples	Potential application
0D	No physical laws	ArcGIS, Delta mapper	Broad scale assessment of flood extents and flood depths
1D	Solution of the 1D equations	Mike 11, HEC-RAS	Design scale modelling, which can be of the order of tens to hundreds of km depending on catchment size
1D+	1D plus a flood storage cell approach flow	Mike 11, HEC-RAS	Design scale modelling, which can be of the order of tens to hundreds of km depending on catchment size, also has the potential for broad scale application if used with sparse cross-sectional data
2D-	2D minus the law of conservation of momentum for the floodplain flow	LISFLOOD-FP,CA model	Large-scale modelling or urban inundation depending on cell dimensions
2D	Solution of the 2D shallow wave equations	TUFLOW, MIKE 21, TELEMAC, DIVAST	Design scale modelling of the order of tens of km. May have the potential for use in broad scale modelling if applied with coarse grids
2D+	2D plus a solution for vertical velocities using continuity only	TELEMAC 3D	Predominantly coastal modelling applications where 3D velocity profiles are important. Has also been applied to reach scale river modelling problems in research projects

Scientists have made several efforts to incorporate uncertainty in hydraulic modelling, flood mapping and inundation analysis (Saleh et al., 2017; Yin and Yu 2016; Smeome et al., 2007; Baldassarre et al. 2009).

In recent years the popularity of 2D hydrodynamic model has increased substantially and TUFLOW (Syme 1992; Huxley 2004; Lhomme et al. 2008; Phillips et al. 2005) is one of the most applied model in this area. The two dimensional (2D) model TUFLOW has its own advantage in solving complex flow pattern in coastal waters, estuaries, rivers and floodplain.

Regardless of where these disasters strike, traffic evacuation is one of the most critical part of emergency preparedness, where evacuees will be transferred from most critical regions to safe regions and the ill and injured will be transported to medical facilities. Traffic evacuation plans and routes must be decided and analyzed, and furthermore transportation infrastructure must be optimized during evacuation to achieve an efficient emergency management response. Based on evacuations data from January, 1990 to June, 2003, the United States (U.S.) Nuclear Regulatory Commission (NRC) claimed that approximately every three weeks there were a large-scale evacuation involving at least 1000 people evacuating the critical regions. These evacuations were ordered due to many reasons, including natural disasters, wildfire, hazardous materials release and terrorist attacks, where natural disaster was the leading issue with 58% of total evacuations. However, a successful evacuation requires organizing the necessary manpower, equipment resources and technological supports available at the right time, at the right place, and in the right quantity. Communication, coordination, and knowledge to make the process work also play important role on the success of traffic evacuation.

Every three years, there are approximately five hurricanes strikes the east coast of U.S, resulting in 50-100 casualties (Schwartz 2007). These hurricanes impact our society in numerous ways. Meanwhile, in 2012 there was a very catastrophic natural disaster along the east coast of the United States of America. This disaster was known as Superstorm Sandy, and it took over 150 lives and caused billions of dollars in structural and property damage (Blake 2013). It was one of the largest and costliest recorded storms to impact the U.S. Northeast. The majority of this damage was associated with infrastructure, including buildings, transportation links and facilities, water retaining structures, and water/wastewater treatment systems. New Jersey's aging and degraded storm water infrastructures threaten to disrupt daily life, commerce and industry, and stunt future economic prosperity. The damage revealed the importance of appropriate preparation and response strategies in the face of extreme weather events (Kar and Hodgson 2008, Hall 2013, Blake 2013, NOAA 2012).

The heterogeneous disasters challenge transportation planners, engineers and emergency managers to estimate the time needed to evacuate people from a threatened area to a safe place in an efficient and smooth manner during hurricanes. Prior estimation of the evacuation time also could be used to identify the evacuation strategies and optimize the existing roadway capacity. It is mandated by the federal government that each state agency have to develop its own evacuation strategies and guidelines before any major hurricanes, cyclones or storms hit the land surface (FEMA 2006a, Kar and Hodgson 2008). These strategies should be evaluated and practiced before to identify the efficiency of these strategies. Moreover, the government agencies are responsible to update strategies in timely manners based on recent experiences. However, there were

still huge delays and log congestions on our roads and highways while evacuating people as failed to optimize the existing transportation structure during evacuation.

Table 7

Traffic evacuation times during recent hurricanes in U.S

Hurricanes	**Year**	**State**	**Mandatory Evacuation Started**	**Evacuation Traffic Flow**
Hurricane Gordon (Category 1)	2000	FL	September 17 (30 hours)	More than 30 hours
Hurricane Katrina (Category 3)	2005	LA, AL	August 28 (40 hours)	Around 30 hours
Hurricane Earl	2010	NC, ME	August 31 (3 days)	Less than 24 hours
Hurricane Irene (Category 1)	2011	NC, SC, NJ, DE, VA, MD	Midnight August 25 (48-72 hours)	Around 20 hours
Superstorm Sandy	2012	NJ, NY, DE, MD	October 27 (2 days)	32 hours
Hurricane Arthur (Category 2)	2014	NC, DE, CT, NJ, NY	Early morning July 3 (24 hours)	12 hours
Hurricane Joaquin (Category 3)	2015	VA, NC, NJ	3:00 PM EDT, October 1 (6 days)	More than 60 hours
Hurricane Matthew (Category 5)	2016	FL, NC, SC	October 4 (4 days)	Around 40 hours

During Hurricane Rita, a 100 miles long queue happened on highways in Huston, Texas and evacuees spent more than 20 hours in traffic congestions. About 100 people

died on roads while evacuating from the coastal regions during Hurricane Rita (Blumenthal 2005, Litman 2006, Zachria and patel 2006, Wu et al. 2012). Lack of proper transportation evacuation plans and strategies were identified responsible for that incident. Based on the response time, the overall evacuation time can vary. Researchers found that only 5% population in critical region will evacuate before an official order, 61% left the day of order and 31% left the day after the order was issued (Dow and Cutter 2002). A complete traffic evacuation during hurricanes can take on an average 2.33 days in U.S. Table 7 shows the traffic evacuation times during recent hurricanes in U.S.

The objective of this study was to develop a 2D hydrodynamic model to assess the extent of flooding due to extreme weather events like superstorm Sandy and using this hydrodynamic model to evaluate the efficiency of existing transportation infrastructure. Furthermore, this evaluation was used to develop a decision-support framework for extreme evacuation planning to prepare the communities living in critical regions.

3.2 Study Area

Brick Township is located in Ocean County, New Jersey, United States (Figure 19). As of the 2010 United States Census, the township had a population of 75,072 making it the state's 13th-largest municipality and the third most populous municipality in Ocean County. According to the United States Census Bureau, the township had a total area of 32.315 square miles, including 25.715 square miles of land and 6.600 square miles of water (20.42%). While the majority of Brick Township is located on the mainland, Ocean Beaches I, II and III are situated on the Barnegat Peninsula, a long, narrow barrier peninsula that separates Barnegat Bay from the Atlantic Ocean.

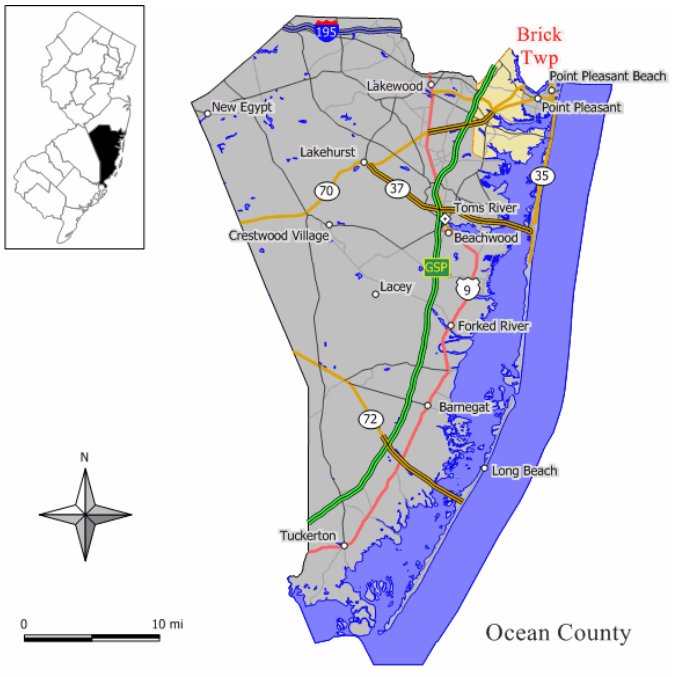

Figure 19. Map of study area (Brick Township)

3.3 Model Description

3.3.1 TUFLOW. The Surface-Water Modeling System (SMS) software is a GIS based system for developing, running, and processing water surface models using a wide variety of river and coastal hydraulics models. SMS is the primary GUI interface for the two-dimensional (2D) hydraulic model TUFLOW that was used to simulate free-surface water flow for urban waterways, rivers, coastlines, etc. The fully 2D solution algorithm of TUFLOW is based on Stelling (1984) and solves the full two-dimensional, depth averaged, momentum and continuity equations for free-surface flow (TUFLOW 2006). TUFLOW is specifically oriented towards establishing flow patterns in coastal waters, estuaries, rivers, floodplains and urban areas where the flow patterns can be accurately modeled using two-dimensional approximations. The solution algorithm of TUFLOW is

based on the depth averaged 2D shallow water equations (SWE). The SWE are the equations of fluid motion used for modelling floods, ocean tides and storm surges. They are derived using the hypotheses of vertically uniform horizontal velocity and negligible vertical acceleration.

The 2D SWE in the horizontal plane are described by the partial differential equations (PDE) of mass continuity and momentum conservation in the X and Y directions in a Cartesian coordinate frame of reference (TUFLOW 2006). The equations are:

$$\frac{\partial \zeta}{\partial t} + \frac{\partial (Hu)}{\partial x} + \frac{\partial (Hv)}{\partial y} = 0 \text{ (2D Continuity)} \quad (3.1)$$

$$\frac{\partial u}{\partial t} + u\frac{\partial u}{\partial x} + v\frac{\partial u}{\partial y} - C_f v + g\frac{\partial \zeta}{\delta x} + gu\left(\frac{n^2}{H^{\frac{4}{3}}} + \frac{f_l}{2g\Delta x}\right)\sqrt{u^2+v^2} - \mu\left(\frac{\partial^2 u}{\partial_{x^2}} + \frac{\partial^2 u}{\partial_{y^2}}\right) + \frac{1}{\rho}\frac{\partial p}{\partial x} =$$

$$F_x \text{ (X momentum)} \quad (3.2)$$

$$\frac{\partial v}{\partial t} + u\frac{\partial v}{\partial x} + v\frac{\partial v}{\partial y} - C_f u + g\frac{\partial \zeta}{\delta x} + gv\left(\frac{n^2}{H^{\frac{4}{3}}} + \frac{f_l}{2g\Delta x}\right)\sqrt{u^2+v^2} - \mu\left(\frac{\partial^2 v}{\partial_{x^2}} + \frac{\partial^2 v}{\partial_{y^2}}\right) + \frac{1}{\rho}\frac{\partial p}{\partial x} =$$

$$F_x \text{ (Y momentum)} \quad (3.3)$$

Where ζ =water surface elevation, u and v =depth averaged velocity components in X and Y directions, H = depth of water, t=time, x and y = distance in X and Y directions, Δx and Δy = cell dimensions in X and Y directions, c_f = Coriolis force coefficient, n = manning's n, f_l= energy loss coefficient, μ= horizontal diffusion of momentum coefficient, p = atmospheric pressure, ρ= density of water, F_x and F_y= sum of components of external forces in X and Y directions. The SWE can be attributed to different physical phenomena such as; propagation of the wave due to gravitational

forces, transport of momentum by advection, external forces such as bed friction, rotation of earth and barometric pressure.

3.3.2 PTV-VISSIM. Due to recent advances in computing power and technologies the computer simulation uses in traffic analysis has become more common. These traffic simulations were calibrated using real world data to mimic the real world and then the outputs from traffic simulations were used as a satisfactory representation of the real world. In this study, PTV VISSIM traffic microsimulation package was utilized for evaluating different evacuation scenarios under different extreme weather events. The main reason behind this selection was its ability to simulate detailed vehicle interactions at specific locations in the transportation network. This software was also used for dynamic rerouting/ detouring the evaluation vehicles because it supported modeling the dynamic interactions between vehicles and transportation infrastructure systems in the Component Object Model (COM).

3.4 Data Collection and Processing

The process for developing the framework is divided into three major components. First, developing the 2D hydrodynamic model to identify the flood depth and flood extent for the evacuation routes. Second, providing the output from hydrodynamic model as an input to the traffic simulation model i.e. which and when certain evacuation route will be closed or open. Third, integrating output from traffic and hydrodynamic simulation to develop dynamic GIS map for public dissemination.

3.4.1 Description of data for TUFLOW simulation. The data required to run a TUFLOW simulation is divided in to four main components.

i) Digital Elevation Model: The digital elevation model (DEM) that was used for SMS-Tuflow was gathered from the United States Geological Survey (USGS) (source: https://nationalmap.gov/3DEP/index.html). The DEM comes from the National Elevation Dataset (NED) which provides elevation raster data for all of United States including territorial islands. The geographical coordinates for the NED are related to the North American Datum of 1983 (NAD 83). All of the elevation data is in meters and related to the North American Vertical Datum of 1988 (NAVD 88). The DEM used for our study was at a 1/3 arc-second resolution which translates to around 10 meters. However, the NED does offer resolutions at 1 arc-second (30 meters) and in limited places they offer 1/9 arc-second (3 meter). The elevation dataset was downloaded as raster file.

ii) Bathymetry data: For proper channel definition a bathymetry was needed to be overlaid upon the DEM data. The bathymetry data was obtained from NOAA (source: http://estuarinebathymetry.noaa.gov/documentation/30m_bathy.html). The geographical coordinates for the NED are related to the North American Datum of 1983 (NAD 83). But the vertical datum was Mean Low Water level (MLW) which was different than the DEM dataset we used. The horizontal and vertical units were in meter. But the resolution of the data was 30m. The data was provided in a raster format.

iii) Landuse/Landcover (LU/LC) data: In order to properly run SMS land use data needs to be overlaid and converted from feature object to polygon and connected to the DEM. The land use data provides a Manning's Number for each surface types. The land use data was gathered from the New Jersey Department of Environmental Protection (NJDEP) by the bureau of geographical information science (GIS). The data was gathered in 2012 and used the categories: Agriculture, Barren Land, Forest, Urban Land,

Water, and Wetlands. Furthermore, the land use data is broken up into 14 regions to cover all of New Jersey. The LU/LC information was provided as a shapefile.

iv) Water level vs time or discharge vs time data: The required water level data as upstream and downstream boundary condition (BC) was obtained from the USGS current water data (source: https://maps.waterdata.usgs.gov/). The duration of the data for those stations was 10/27/2012 to 10/31/2012. Detailed information of the stations are given in the Table 8.

Table 8

Observed water level vs time data for TUFLOW boundary condition

Site Number	Site Name	Type of data	Temporal resolution	Upstream/Downstream BC	Datum
USGS 01408168	Barnegat Bay at Mantoloking, NJ	Gage height(ft) vs time	6 min	Upstream	NAVD* 1988
USGS 01408050	Manasquan River at Point Pleasant NJ	Gage height(ft) vs time	6min	Upstream	NAVD* 1988
USGS 01408120	North Branch Metedeconk	Gage height(ft) vs time	15 min	Downstream	NGVD* 1929
USGS 01408029	Manasquan River near Allenwood NJ	Gage height(ft) vs time	15 min	Downstream	NGVD* 1929

Note. *NAVD: North American vertical Datum *NGVD: National Geodetic Vertical Datum

3.4.2 Pre-processing of the data.

3.4.2.1 Merging of DEM and bathymetry data. In order to run a TUFLOW simulation the DEM must be merged with the bathymetry data for accurate representation of channel cross-section. The bathymetry data was resampled to 10 m using bilinear interpolation in ArcGIS to match with the resolution of the USGS 10 m DEM data. For a consistent vertical datum, the resampled bathymetry data was converted from MLW datum to NAVD 1988 vertical datum using a tool developed by NOAA called 'Vdatum' (Parker et al. 2003). After that, both the bathymetry and the DEM data were merged to a new raster file. A raster conversion was performed to convert the elevation data from meter to feet. and imported into SMS interface. The final output is shown in Figure 20.

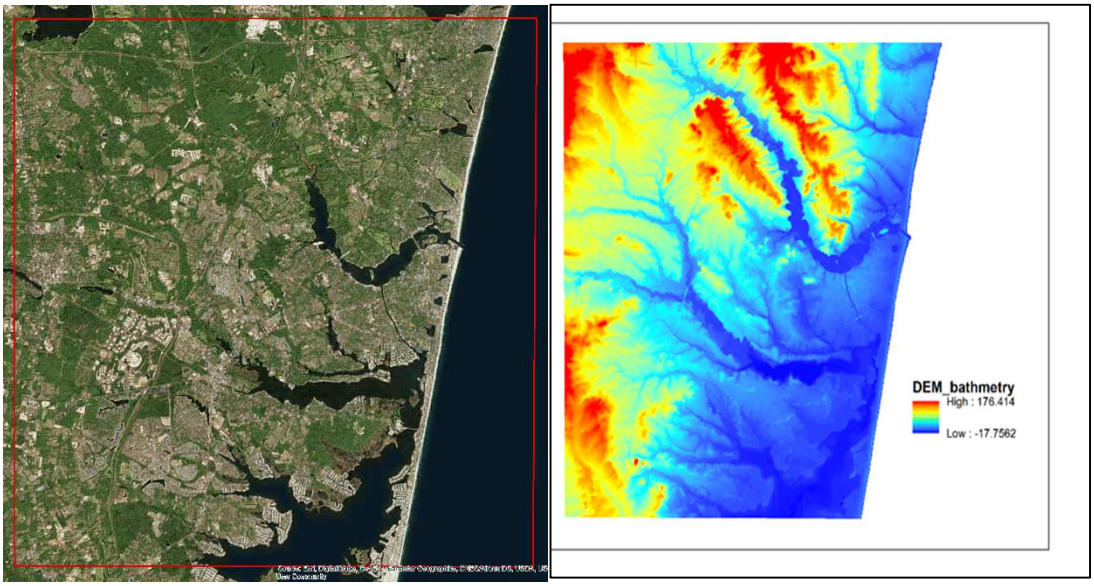

Figure 20. Merging DEM and bathymetry data

3.4.2.2 LU/LC data processing. The LU/LC data we used was provided for all Ocean County in NJ. In order for easier and faster data processing in SMS we clipped that LU/LC data according to our study area over Brick Township. Also, the projection transformation was performed for this LU/LC shapefile data from State plane coordinate system to NAD 1983 datum. Figure 21 depicts the land use classification for our study area. Most of the area consists of urban area. There are some wetlands around the main channel and in the north part of the study area.

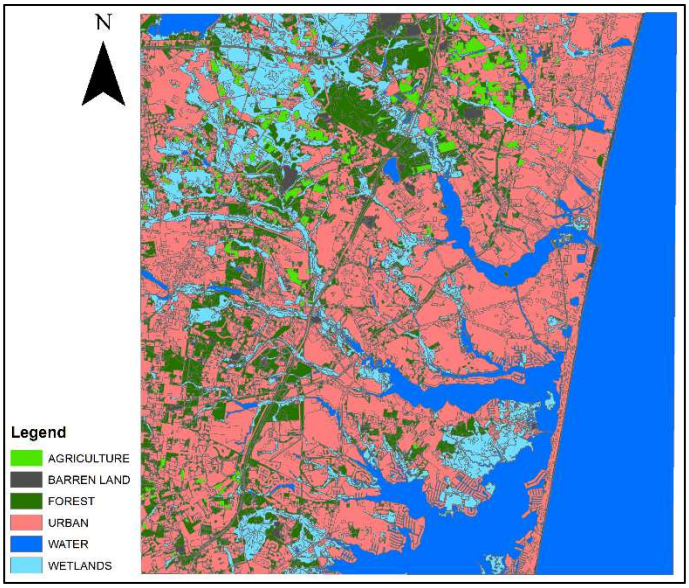

Figure 21. Land use classification

3.4.2.3 Water level data processing. We used water level (ft) vs time as our boundary condition (BC) in SMS- TUFLOW as shown in Figure 22. First the raw data

was converted to averaged hourly value according to our duration of simulation. Also, the datum adjustment was performed from NGVD to NAVD for a consistent vertical datum.

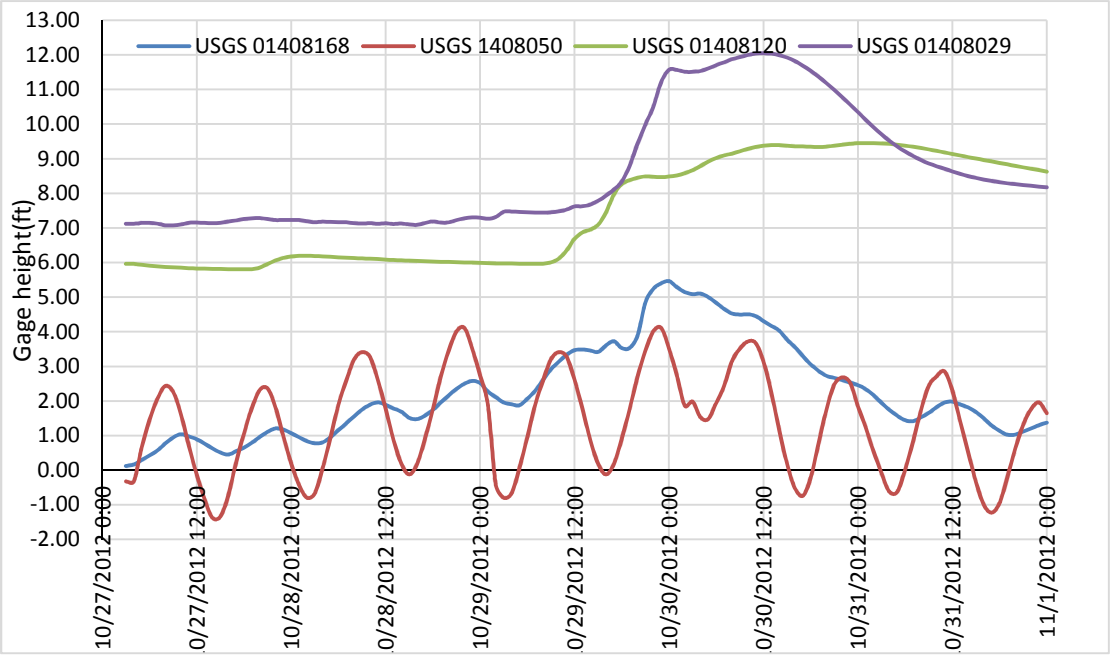

Figure 22. Hourly water level data for upstream and downstream BC

3.4.3 Processing in SMS. All of the DEM, bathymetry, land use data were imported in to SMS interface for he hydrodynamic modelling. An important step in SMS was to defining the mesh size. The cell sizes of 2D domains need to be sufficiently small to reproduce the hydraulic behavior, yet be large enough to minimize run times to meet project deadlines. Preferably at least three to four cells across the major flow paths is recommended. Considering all these, we used a cell size of 10m for faster computing. The selection of time step is also a crucial parameter for accurate hydrodynamic modelling which ensures a stable TUFLOW simulation. The run time is directly proportional to the number of timesteps required to calculate model behavior for the

simulation period, while the computations may become unstable and meaningless if the timestep is greater than a limiting value. As a general rule, the timestep (in seconds) is typically in the range of 1⁄2 to 1⁄5 of the cell size (in meters). For a 10m model the timestep will typical be in the range 2 – 5 seconds. For steep models with high Froude numbers and supercritical flow, smaller timesteps may be required. It is strongly advised to not simply reduce the timestep if the model is unstable, but rather to establish why it is unstable and, in most instances, correct or adjust the model topography, initial conditions or boundary conditions to correct the instability. For our analysis we used 4 second as our time step. The duration of our simulation was from 10/27/2012 0:00 to 10/31/2012 0:00. The hurricane sandy made the landfall during 10/29/2012 near Atlantic City, NJ.

3.4.4 Evacuation traffic network modeling. We conducted a thorough literature review on traffic evacuation to identify the current practices and strategies for extreme weather events in the selected study region, Brick Township. Furthermore, the critical regions and the location of shelters, hence the origins and destinations were established based on the literature review. The next step was to code the detailed microsimulation model of the existing transportation infrastructure, which was the base model for entire study, and then release the evacuation traffic on the road networks for various flood scenarios. The evacuation traffic was predicted based on the Annual Average Daily Traffic (AADT) values in 2012-13 collected from NJDOT websites. Figure 23 shows the traffic evacuation model developed using Vissim software.

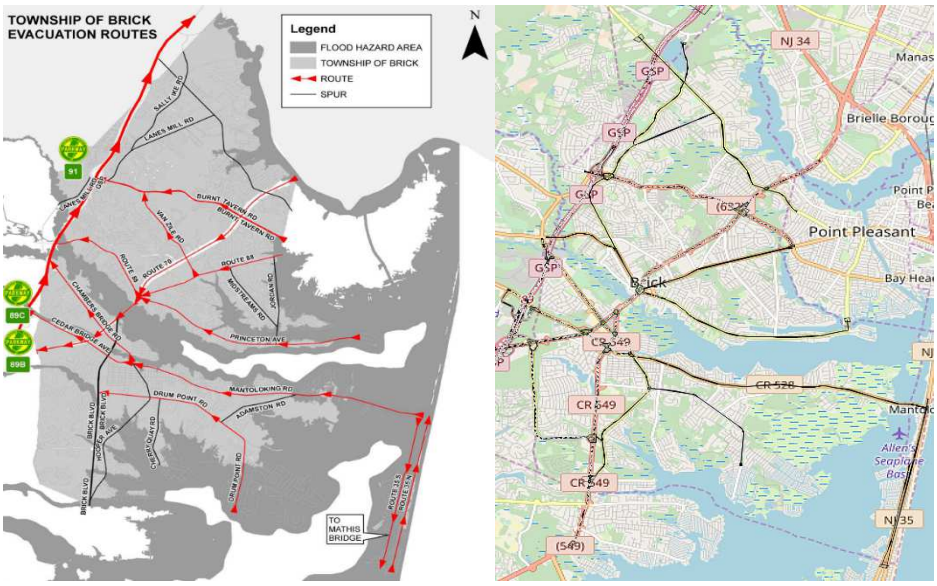

Figure 23. Traffic Evacuation Network of Brick Township; Collected Evacuation Route (Left) and Microsimulation Model (Right)

This base model was calibrated later using the data collected from the field, i.e. travel time, and turning percentages. Travel time were used to calibrate the simulation model because it was a common performance measures used in traffic studies. The travel times were collected from filed data collections at four road segments of Brick Township (selected road segments are presented in Figure 24), covering at least 10% of the length of the total road networks, and compared to travel times that occurred during simulation iterations at the same road segments. The model was considered to accurately represent the real-world scenario because it was less than ten percent of the observed values.

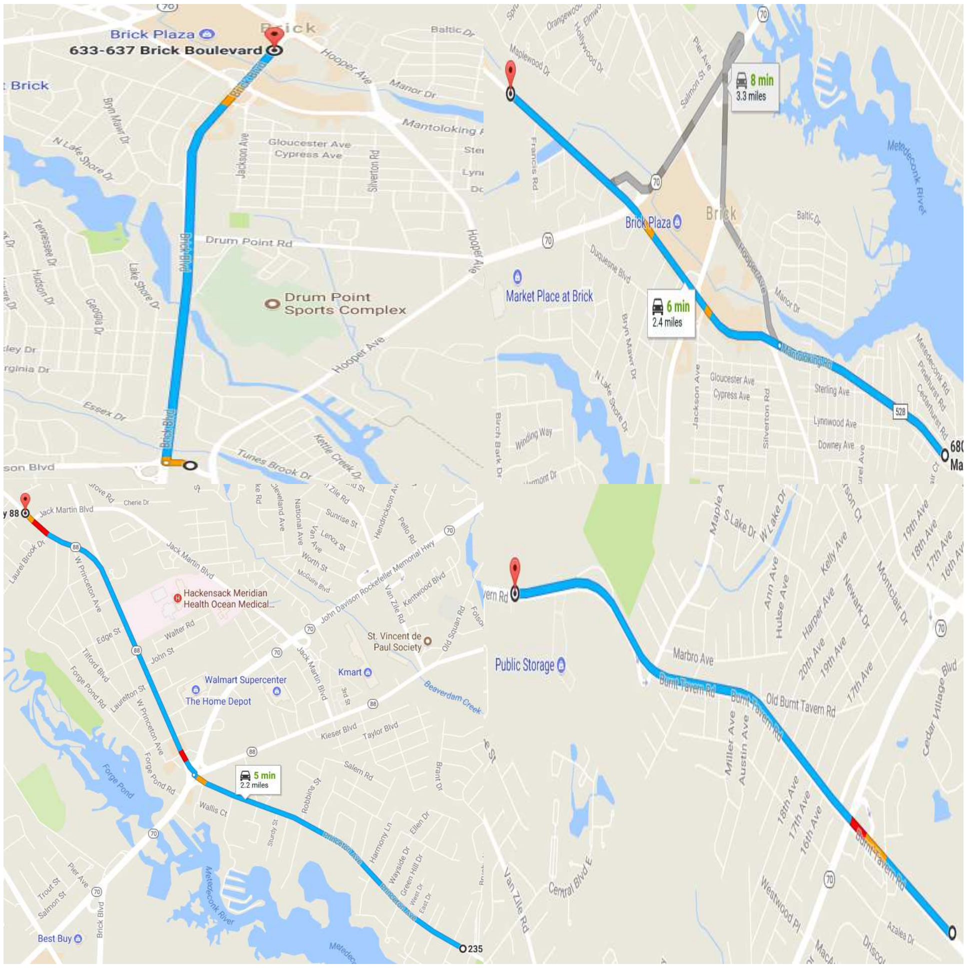

Figure 24. Calibration Segments for traffic simulation

3.4.5 Integration of hydrodynamic and traffic evacuation models. The results of 2D hydrodynamic models were then integrated into traffic evacuation models using a code that was controlled by Visual Studio 2015. Based on the predicted water surge level, the future availability of a road segment was computed in hydrodynamic model and this information was passed to Vissim model. Later, these information were utilized to detour the evacuating traffics ahead of time. The detour routing coded based on the suggestions provided in Interactive Detour Route Mapping (IDRuM) application. This web-based

application was developed by the joint venture of Delaware Valley Regional Planning Commission (DVRPC) and Pennsylvania Department of Transportation (Penn DOT). The updates in the evacuation traffic flow could optimize the usage of the existing transportation infrastructures and hence, reduce the overall network evacuation travel time. The network travel time for each 15 minutes were recorded. The integration algorithms used in this research are presented in Figure 25.

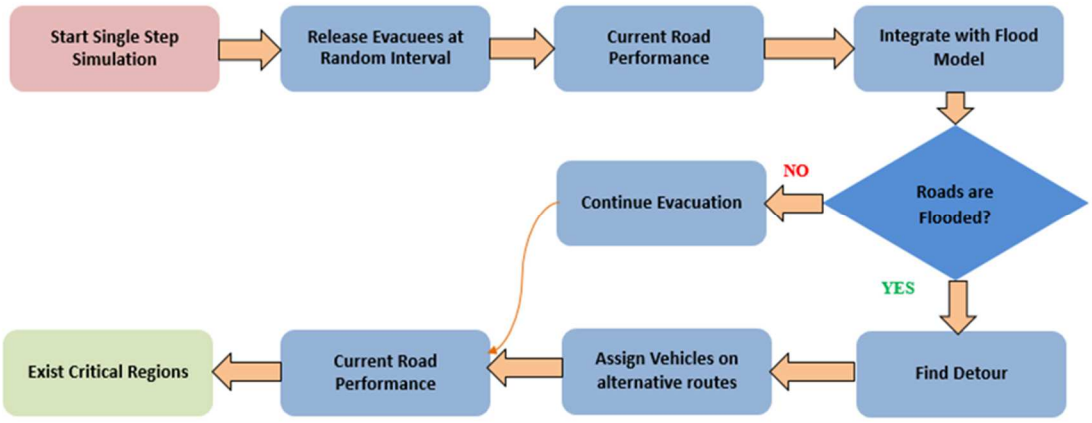

Figure 25. Integration algorithms to combine hydrodynamic and traffic simulation

3.5 Results and Discussion

The results of the hydrodynamic and traffic simulation models could be divided into two sub-sections. However, the final results, i.e. evacuation traffic velocity distribution were sketched on Google Earth map. This maps can be a useful tool for the coastal communities about when to evacuate, which routes are suitable for evacuation

and to decide which alternative routes people needs to choose during emergency evacuation.

3.5.1 Outputs from flood modeling. From TUFLOW simulation we estimated the height of water level with respect to time in our study area, Brick Township. The highest water level inland was ~8.0 ft as shown in Figure 26.

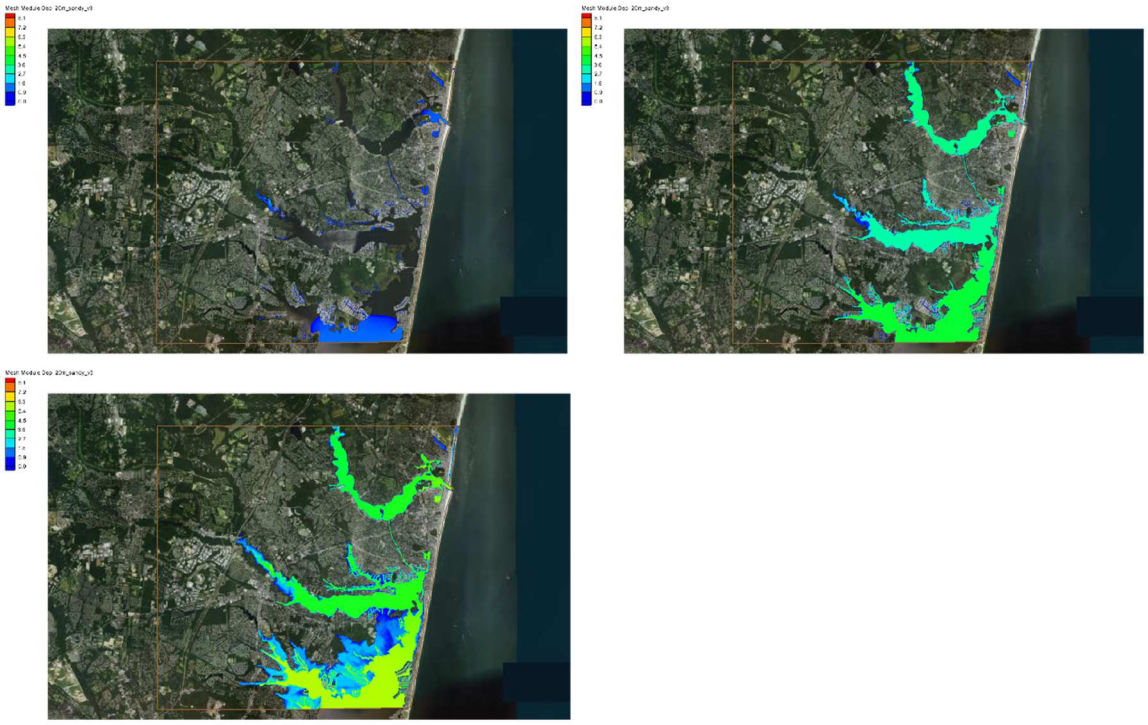

Figure 26. Flooding in Brick Township at different time interval during superstorm Sandy as simulated by TUFLOW

Also, the southern part of Brick Township was affected most due to the flooding. Using the flooding information from simulation we identified which roads will be

affected due to flooding. We also identified when the roads would be affected and what would be the flood level at certain location on evacuation routes. All of this information was exported into the traffic simulation models. Using that, what-if scenarios were created for the evacuation routes.

3.5.2 Outputs from evacuation modelling. Using evacuation traffic models, the performance of the existing transportation infrastructure was evaluated. To evaluate performance, the times required to evacuate from critical regions to a safe zone were estimated while running microsimulation.

Figure 27. Bottleneck formation after announcement of Mandatory Evacuation; a) 02:00 hours of simulation (left) and b) 06:00 hours of simulation (right)

Hydrodynamic models were integrated with traffic evacuation models. Using flood prediction algorithms hydrodynamic models sent the information on future status of any specific roadway segments. This information was passed to vissim traffic evacuation

model using Visual Basic code. First we simulated the models without re-routing the vehicles into alternative routes. After 6:00 hours of simulation, it was found that three additional numbers of bottleneck zone were formed with compared to 2 hours of simulation. The locations of these bottlenecks were presented in Figure 27. Finally the alternative routing provided in IDRuM web application were modeled in traffic simulations. Later outputs from flood modeling for same category hurricane used earlier were integrated in traffic simulation models. The alternative routing information were then utilized to optimize the capacity of the existing road structure and distribute the evacuating traffic among the less congested road segment. This optimization led to reduction of the overall travel time of about 6% compared to base model. The detailed comparison is presented in Figure 28.

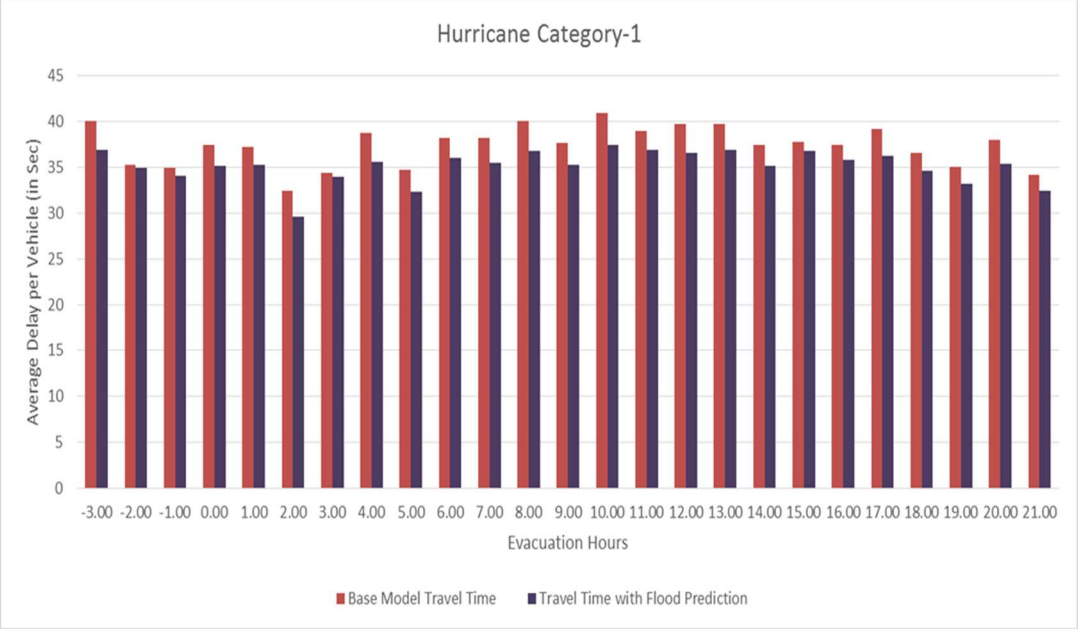

Figure 28. Comparison of Travel Times between Base Model and Model with Flood Prediction Information

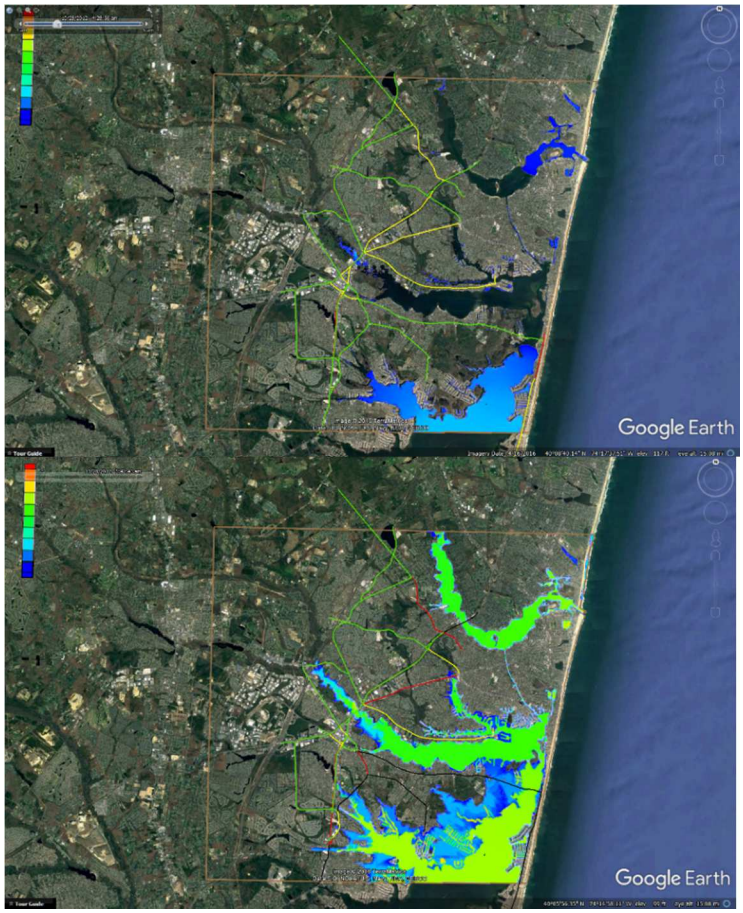

Figure 29. Final evacuation planning based on traffic map

Furthermore, the velocity distribution, generated from traffic simulation models, was plotted on Google Earth map (Figure 29). As we can see from Figure 29 before flood is approaching all evacuation routes were open after two hours of simulation and traffic velocity was varied in between 5~25 mph (referred as yellow line in Figure 29) and 25~50 mph (referred as green line). As flood was approaching in the 2nd picture certain routes were closed. The transportation infrastructure were also became congested due to the segments of road network were shut down.

3.6 Conclusion

The inundation maps produced from fine scale flood simulations are induced with uncertainties through data collection, model development, numerical simulation and theoretical assumption which results inaccurate and ultimately misleading information. Bales and Wagner (2009) mentioned that currently uncertainties in inundation maps are left unspecified. Model calibration process includes the parameterization of roughness coefficient to minimize the error between observation and prediction by assuming only one optimum set of coefficients. However, Aronica and Beven (1998) concluded that there could be several optimum parameter sets due to the non-linearity of flood models. To address this issue Pappenberger et al. (2004) performed Monte Carlo simulations by utilizing generalized likelihood uncertainty estimation (GLUE) procedure. One of the most important data sources of model development of fine scale flood modeling is topography derived from LIDAR which typically has a vertical accuracy of ±15 cm (Mason et al. 2003). Werner (2001) investigated the impact of DEM grid size on flood extent mapping and found significant increase in inundation ranging from 10% to 26%. Another source of uncertainty arises from using the flood hydrograph. The implication of gradually varied flow assumption in flood modelling could over predict the inundation area at higher discharges due to the time required to reach a steady condition. This time typically exceeds the total volume and duration of the peak discharge present in a flood hydrograph (Bales and Wagner 2009). Thus more accurate representation of topography, proper model parameterization and boundary condition could certainly improve the models performance in reducing the uncertainty. The integration of hydrodynamic and transportation modeling could help to evaluate real world extreme weather event

evacuation strategies. This integration also could be used in the evacuation situations where the segments of road network are closed due to flooding. The optimization of evacuation traffic movements could lead to reduction in the overall evacuation travel time. Using that information the related agencies or departments can select alternate routes for efficient evacuation. Furthermore, this type of combination between hydrodynamic modelling and traffic modelling can provide useful information to the communities, agencies as well as decision makers for an optimum and useful emergency evacuation planning during extreme storm events.

References

[1] C. D. Huxley, "TUFLOW Testing and Validation," *Griffith University, Brisbane,* 2004.

[2] A. V. Ines and J. W. Hansen, "Bias correction of daily GCM rainfall for crop simulation studies," *Agricultural and forest meteorology,* vol. 138, pp. 44-53, 2006.

[3] M. Jakob Themeßl, A. Gobiet, and A. Leuprecht, "Empirical-statistical downscaling and error correction of daily precipitation from regional climate models," *International Journal of Climatology,* vol. 31, pp. 1530-1544, 2011.

[4] C. P. Jelesnianski, J. Chen, and W. A. Shaffer, "SLOSH: Sea, lake, and overland surges from hurricanes," 1992.

[5] C. Jones, J. Hughes, N. Bellouin, S. Hardiman, G. Jones, J. Knight*, et al.*, "The HadGEM2-ES implementation of CMIP5 centennial simulations," *Geoscientific Model Development,* vol. 4, p. 543, 2011.

[6] B. Kar and M. E. Hodgson, "A GIS-based model to determine site suitability of emergency evacuation shelters," *Transactions in GIS,* vol. 12, pp. 227-248, 2008.

[7] T. R. Karl, R. W. Knight, D. R. Easterling, and R. G. Quayle, "Indices of climate change for the United States," *Bulletin of the American Meteorological Society,* vol. 77, pp. 279-292, 1996.

[8] T. R. Karl and R. W. Knight, "Secular trends of precipitation amount, frequency, and intensity in the United States," *Bulletin of the American Meteorological society,* vol. 79, pp. 231-241, 1998.

[9] A. I. McLeod, "Kendall rank correlation and Mann-Kendall trend test," *R Package Kendall,* 2005.

[10] K. Krivoruchko, *Spatial statistical data analysis for GIS users*: Esri Press Redlands, 2011.

[11] L. M. Kueppers, M. A. Snyder, L. C. Sloan, E. S. Zavaleta, and B. Fulfrost, "Modeled regional climate change and California endemic oak ranges," *Proceedings of the National Academy of Sciences of the United States of America,* vol. 102, pp. 16281-16286, 2005.

[12] C. W. Landsea and J. L. Franklin, "Atlantic hurricane database uncertainty and presentation of a new database format," *Monthly Weather Review,* vol. 141, pp. 3576-3592, 2013.

[13] J. Lhomme, P. Sayers, B. Gouldby, P. Samuels, M. Wills, and J. Mulet-Marti, "Recent development and application of a rapid flood spreading method," 2008.

[14] T. Litman, "Lessons from Katrina and Rita: What major disasters can teach transportation planners," *Journal of Transportation Engineering,* vol. 132, pp. 11-18, 2006.

[15] V. Lucarini, S. Pascale, and J. Böhner, "Seasonality of the hydrological cycle in major South and Southeast Asian river basins as simulated by PCMDI/CMIP3 experiments," *arXiv preprint arXiv:1312.5727,* 2013.

[16] D. M. Ludlum, *The New Jersey Weather Book*: Rutgers University Press, 1983.

[17] R. A. Luettich Jr, J. J. Westerink, and N. W. Scheffner, "ADCIRC: An Advanced Three-Dimensional Circulation Model for Shelves, Coasts, and Estuaries. Report 1. Theory and Methodology of ADCIRC-2DDI and ADCIRC-3DL," COASTAL ENGINEERING RESEARCH CENTER VICKSBURG MS1992.

[18] R. Luettich and J. Westerink, "ADCIRC: A parallel advanced circulation model for oceanic, coastal and estuarine waters; users manual for version 45.08," ed, 2006.

[19] D. Maraun, F. Wetterhall, A. Ireson, R. Chandler, E. Kendon, M. Widmann*, et al.*, "Precipitation downscaling under climate change: Recent developments to bridge the gap between dynamical models and the end user," *Reviews of Geophysics,* vol. 48, 2010.

[20] D. C. Mason, D. M. Cobby, M. S. Horritt, and P. D. Bates, "Floodplain friction parameterization in two-dimensional river flood models using vegetation heights derived from airborne scanning laser altimetry," *Hydrological processes,* vol. 17, pp. 1711-1732, 2003.

[21] S. McGinnis, D. Nychka, and L. O. Mearns, "A new distribution mapping technique for climate model bias correction," in *Machine learning and data mining approaches to climate science*, ed: Springer, 2015, pp. 91-99.

[22] G. A. Meehl, C. Covey, K. E. Taylor, T. Delworth, R. J. Stouffer, M. Latif*, et al.*, "The WCRP CMIP3 multimodel dataset: A new era in climate change research," *Bulletin of the American Meteorological Society,* vol. 88, pp. 1383-1394, 2007.

[23] P. Melchior, "The tides of the planet Earth," *Organic Photonics and Photovoltaics,* 1983.

[24] A. Moberg and P. D. Jones, "Trends in indices for extremes in daily temperature and precipitation in central and western Europe, 1901–99," *International Journal of climatology,* vol. 25, pp. 1149-1171, 2005.

[25] K. Sullivan and L. Uccellini, "Service assessment: Hurricane/post-tropical cyclone Sandy, October 22–29, 2012," *US Department of Commerce NOAA and NWS, Silver Spring, Maryland,* vol. 66, 2013.

[26] T. Ogata, H. Ueda, T. Inoue, M. Hayasaki, A. Yoshida, S. Watanabe*, et al.*, "Projected future changes in the Asian monsoon: a comparison of CMIP3 and CMIP5 model results," *Journal of the Meteorological Society of Japan. Ser. II,* vol. 92, pp. 207-225, 2014.

[27] B. Önöz and M. Bayazit, "The power of statistical tests for trend detection," *Turkish Journal of Engineering and Environmental Sciences,* vol. 27, pp. 247-251, 2003.

[28] R. Ortiz, K. D. Sayre, B. Govaerts, R. Gupta, G. Subbarao, T. Ban*, et al.*, "Climate change: can wheat beat the heat?," *Agriculture, Ecosystems & Environment,* vol. 126, pp. 46-58, 2008.

[29] F. Pappenberger, K. Beven, M. Horritt, and S. Blazkova, "Uncertainty in the calibration of effective roughness parameters in HEC-RAS using inundation and downstream level observations," *Journal of Hydrology,* vol. 302, pp. 46-69, 2005.

[30] B. Parker, D. Milbert, K. Hess, and S. Gill, "National VDatum–The implementation of a national vertical datum transformation database," in *Proceeding from the US Hydro'2003 Conference*, 2003, pp. 24-27.

[31] G. Pender, "Briefing: Introducing the flood risk management research consortium," in *Proceedings of the Institution of Civil Engineers-Water Management*, 2006, pp. 3-8.

[32] G. P. Peters, R. M. Andrew, T. Boden, J. G. Canadell, P. Ciais, C. Le Quéré*, et al.*, "The challenge to keep global warming below 2 C," *Nature Climate Change,* vol. 3, p. 4, 2012.

[33] B. Phillips, S. Yu, G. Thompson, and N. De Silva, "1D and 2D Modelling of Urban Drainage Systems using XP-SWMM and TUFLOW," in *10th International Conference on Urban Drainage*, 2005, pp. 21-26.

[34] E. S. Poloczanska, C. J. Brown, W. J. Sydeman, W. Kiessling, D. S. Schoeman, P. J. Moore*, et al.*, "Global imprint of climate change on marine life," *Nature Climate Change,* vol. 3, p. 919, 2013.

[35] A. Rammig, T. Jupp, K. Thonicke, B. Tietjen, J. Heinke, S. Ostberg*, et al.*, "Estimating the risk of Amazonian forest dieback," *New Phytologist,* vol. 187, pp. 694-706, 2010.

[36] K. Riahi, S. Rao, V. Krey, C. Cho, V. Chirkov, G. Fischer*, et al.*, "RCP 8.5—A scenario of comparatively high greenhouse gas emissions," *Climatic Change,* vol. 109, p. 33, 2011.

[37] R. O. Gilbert, *Statistical methods for environmental pollution monitoring*: John Wiley & Sons, 1987.

[38] D. A. Robinson, "J2. 1 THE NEW JERSEY WEATHER AND CLIMATE NETWORK: PROVIDING ENVIRONMENTAL INFORMATION FOR A MYRIAD OF APPLICATIONS," 2005.

[39] C. Rosenzweig, W. D. Solecki, L. Parshall, M. Chopping, G. Pope, and R. Goldberg, "Characterizing the urban heat island in current and future climates in New Jersey," *Global Environmental Change Part B: Environmental Hazards,* vol. 6, pp. 51-62, 2005.

[40] O. E. Sala, F. S. Chapin, J. J. Armesto, E. Berlow, J. Bloomfield, R. Dirzo*, et al.*, "Global biodiversity scenarios for the year 2100," *science,* vol. 287, pp. 1770-1774, 2000.

[41] F. Saleh, V. Ramaswamy, Y. Wang, N. Georgas, A. Blumberg, and J. Pullen, "A multi-scale ensemble-based framework for forecasting compound coastal-riverine flooding: The Hackensack-Passaic watershed and Newark Bay," *Advances in Water Resources,* vol. 110, pp. 371-386, 2017.

[42] W. Schlenker, W. M. Hanemann, and A. C. Fisher, "Will US agriculture really benefit from global warming? Accounting for irrigation in the hedonic approach," *American Economic Review,* vol. 95, pp. 395-406, 2005.

[43] U. Schulzweida, L. Kornblueh, and R. Quast, "CDO user's guide," *Climate Data Operators, Version,* vol. 1, 2006.

[44] P. Schureman, "Manual of harmonic analysis and prediction of tides," 1958.

[45] R. Schwartz, *Hurricanes and the Middle Atlantic states*: Blue Diamond Books, 2007.

[46] A. Sebastian, J. Proft, J. C. Dietrich, W. Du, P. B. Bedient, and C. N. Dawson, "Characterizing hurricane storm surge behavior in Galveston Bay using the SWAN+ ADCIRC model," *Coastal Engineering,* vol. 88, pp. 171-181, 2014.

[47] P. Q. Seguí, A. Ribes, E. Martin, F. Habets, and J. Boé, "Comparison of three downscaling methods in simulating the impact of climate change on the hydrology of Mediterranean basins," *Journal of Hydrology,* vol. 383, pp. 111-124, 2010.

[48] P. K. Sen, "Estimates of the regression coefficient based on Kendall's tau," *Journal of the American statistical association,* vol. 63, pp. 1379-1389, 1968.

[49] Y. P. Sheng, "Evolution of a three-dimensional curvilinear-grid hydrodynamic model for estuaries, lakes and coastal waters: CH3D," in *Estuarine and coastal modeling*, 1990, pp. 40-49.

[50] Y. P. Sheng, "On modeling three-dimensional estuarine and marine hydrodynamics," in *Elsevier oceanography series*. vol. 45, ed: Elsevier, 1987, pp. 35-54.

[51] Y. Sheng, V. Alymov, V. Paramygin, and J. Davis, "An integrated modeling system for forecasting of storm surge and coastal inundation," *Estuarine and coastal modeling IX, ML Spaulding, ed., ASCE, Reston, VA,* pp. 585-602, 2006.

[52] W. C. Skamarock, J. B. Klemp, J. Dudhia, D. O. Gill, D. M. Barker, W. Wang*, et al.*, "A description of the advanced research WRF version 2," National Center For Atmospheric Research Boulder Co Mesoscale and Microscale Meteorology Div2005.

[53] C. M. Smemoe, E. J. Nelson, A. K. Zundel, and A. W. Miller, "Demonstrating floodplain uncertainty using flood probability maps," *JAWRA Journal of the American Water Resources Association,* vol. 43, pp. 359-371, 2007.

[54] S. Solomon, *Climate change 2007-the physical science basis: Working group I contribution to the fourth assessment report of the IPCC* vol. 4: Cambridge university press, 2007.

[55] K. Sperber, H. Annamalai, I.-S. Kang, A. Kitoh, A. Moise, A. Turner*, et al.*, "The Asian summer monsoon: an intercomparison of CMIP5 vs. CMIP3 simulations of the late 20th century," *Climate Dynamics,* vol. 41, pp. 2711-2744, 2013.

[56] G. S. Stelling, "On the construction of computational methods for shallow water flow problems," 1983.

[57] B. Stevens, M. Giorgetta, M. Esch, T. Mauritsen, T. Crueger, S. Rast, *et al.*, "Atmospheric component of the MPI-M Earth System Model: ECHAM6," *Journal of Advances in Modeling Earth Systems,* vol. 5, pp. 146-172, 2013.

[58] T. F. Stocker, D. Qin, G. Plattner, M. Tignor, S. Allen, J. Boschung, *et al.*, "Climate change 2013: the physical science basis. Intergovernmental panel on climate change, working group I contribution to the IPCC fifth assessment report (AR5)," *New York,* 2013.

[59] W. J. Syme, "Dynamically linked two-dimensional/one-dimensional hydrodynamic modelling program for rivers, estuaries & coastal waters," 1992.

[60] H. Tang, S. Kraatz, K. Qu, G. Chen, N. Aboobaker, and C. Jiang, "High-resolution survey of tidal energy towards power generation and influence of sea-level-rise: A case study at coast of New Jersey, USA," *Renewable and Sustainable Energy Reviews,* vol. 32, pp. 960-982, 2014.

[61] L. Alexander, X. Zhang, T. Peterson, J. Caesar, B. Gleason, A. Klein Tank, *et al.*, "Global observed changes in daily climate extremes of temperature and precipitation," *Journal of Geophysical Research: Atmospheres,* vol. 111, 2006.

[62] C. Amante, "ETOPO1 1 arc-minute global relief model: procedures, data sources and analysis," *http://www. ngdc. noaa. gov/mgg/global/global. html,* 2009.

[63] G. Aronica, B. Hankin, and K. Beven, "Uncertainty and equifinality in calibrating distributed roughness coefficients in a flood propagation model with limited data," *Advances in water resources,* vol. 22, pp. 349-365, 1998.

[64] P. Bacopoulos and S. C. Hagen, "The intertidal zones of the South Atlantic Bight and their local and regional influence on astronomical tides," *Ocean Modelling,* vol. 119, pp. 13-34, 2017.

[65] J. Bales and C. Wagner, "Sources of uncertainty in flood inundation maps," *Journal of Flood Risk Management,* vol. 2, pp. 139-147, 2009.

[66] S. Balica, N. G. Wright, and F. van der Meulen, "A flood vulnerability index for coastal cities and its use in assessing climate change impacts," *Natural hazards,* vol. 64, pp. 73-105, 2012.

[67] G. Di Baldassarre, G. Schumann, P. D. Bates, J. E. Freer, and K. J. Beven, "Flood-plain mapping: a critical discussion of deterministic and probabilistic approaches," *Hydrological Sciences Journal–Journal des Sciences Hydrologiques,* vol. 55, pp. 364-376, 2010.

[68] P. M. Bartier and C. P. Keller, "Multivariate interpolation to incorporate thematic surface data using inverse distance weighting (IDW)," *Computers & Geosciences,* vol. 22, pp. 795-799, 1996.

[69] L. Beevers, W. Douven, H. Lazuardi, and H. Verheij, "Cumulative impacts of road developments in floodplains," *Transportation research part D: transport and environment,* vol. 17, pp. 398-404, 2012.

[70] M. Bentsen, I. Bethke, J. Debernard, T. Iversen, A. Kirkevåg, Ø. Seland*, et al.*, "The Norwegian Earth system model, NorESM1-M—Part 1: Description and basic evaluation of the physical climate," *Geosci. Model Dev,* vol. 6, pp. 687-720, 2013.

[71] B. Bhaskaran, A. Ramachandran, R. Jones, and W. Moufouma-Okia, "Regional climate model applications on sub-regional scales over the Indian monsoon region: The role of domain size on downscaling uncertainty," *Journal of Geophysical Research: Atmospheres,* vol. 117, 2012.

[72] C. A. Blain and W. Rogers, "Coastal tide prediction using the ADCIRC-2DDI hydrodynamic finite element model: Model validation and sensitivity analyses in the Southern North Sea/English Channel," NAVAL RESEARCH LAB STENNIS SPACE CENTER MS COASTAL AND SEMI-ENCLOSED SEAS SECTION1998.

[73] C. A. Blain, R. S. Linzell, and T. C. Massey, "MeshGUI: A mesh generation and editing toolset for the ADCIRC model," NAVAL RESEARCH LAB STENNIS SPACE CENTER MS OCEANOGRAPHY DIV2008.

[74] E. S. Blake, T. B. Kimberlain, R. J. Berg, J. P. Cangialosi, and J. L. Beven Ii, "Tropical cyclone report: Hurricane sandy," *National Hurricane Center,* vol. 12, pp. 1-10, 2013.

[75] R. Blumenthal, "Miles of traffic as Texans heed order to leave," *New York Times,* vol. 23, 2005.

[76] K. Buchholz and R. Zampella, "A 30-year fire history of the New Jersey Pine Plains," *Bull. New Jersey Acad. Sci,* vol. 32, pp. 61-69, 1987.

[77] E. Buonomo, R. Jones, C. Huntingford, and J. Hannaford, "On the robustness of changes in extreme precipitation over Europe from two high resolution climate change simulations," *Quarterly Journal of the Royal Meteorological Society,* vol. 133, pp. 65-81, 2007.

[78] V. Casulli and R. A. Walters, "An unstructured grid, three-dimensional model based on the shallow water equations," *International journal for numerical methods in fluids,* vol. 32, pp. 331-348, 2000.

[79] G. Choi, D. Collins, G. Ren, B. Trewin, M. Baldi, Y. Fukuda*, et al.*, "Changes in means and extreme events of temperature and precipitation in the Asia-Pacific Network region, 1955–2007," *International Journal of Climatology,* vol. 29, pp. 1906-1925, 2009.

[80] J. H. Christensen, T. R. Carter, M. Rummukainen, and G. Amanatidis, "Evaluating the performance and utility of regional climate models: the PRUDENCE project," ed: Springer, 2007.

[81] J. H. Christensen, F. Boberg, O. B. Christensen, and P. Lucas-Picher, "On the need for bias correction of regional climate change projections of temperature and precipitation," *Geophysical Research Letters,* vol. 35, 2008.

[82] M. A. Cialone, A. S. Grzegorzewski, D. J. Mark, M. A. Bryant, and T. C. Massey, "Coastal-storm model development and water-level validation for the North Atlantic Coast Comprehensive Study," *Journal of Waterway, Port, Coastal, and Ocean Engineering,* vol. 143, p. 04017031, 2017.

[83] M. Collins, R. Knutti, J. Arblaster, J.-L. Dufresne, T. Fichefet, P. Friedlingstein, *et al.*, "Long-term climate change: projections, commitments and irreversibility," 2013.

[84] R. E. Davis and R. Dolan, "Nor'easters," *American Scientist,* vol. 81, pp. 428-439, 1993.

[85] J. C. Dietrich, S. Tanaka, J. J. Westerink, C. Dawson, R. Luettich, M. Zijlema, *et al.*, "Performance of the unstructured-mesh, SWAN+ ADCIRC model in computing hurricane waves and surge," *Journal of Scientific Computing,* vol. 52, pp. 468-497, 2012.

[86] N. S. Diffenbaugh, T. W. Hertel, M. Scherer, and M. Verma, "Response of corn markets to climate volatility under alternative energy futures," *Nature climate change,* vol. 2, p. 514, 2012.

[87] R. M. Doherty, L. O. Mearns, K. R. Reddy, M. W. Downton, and L. McDaniel, "Spatial scale effects of climate scenarios on simulated cotton production in the southeastern USA," *Climatic Change,* vol. 60, pp. 99-129, 2003.

[88] C. A. Dos Santos, C. M. Neale, T. V. Rao, and B. B. da Silva, "Trends in indices for extremes in daily temperature and precipitation over Utah, USA," *International Journal of Climatology,* vol. 31, pp. 1813-1822, 2011.

[89] K. Dow and S. L. Cutter, "Emerging hurricane evacuation issues: hurricane Floyd and South Carolina," *Natural hazards review,* vol. 3, pp. 12-18, 2002.

[90] J.-L. Dufresne, M.-A. Foujols, S. Denvil, A. Caubel, O. Marti, O. Aumont, *et al.*, "Climate change projections using the IPSL-CM5 Earth System Model: from CMIP3 to CMIP5," *Climate Dynamics,* vol. 40, pp. 2123-2165, 2013.

[91] J. P. Dunne, J. G. John, A. J. Adcroft, S. M. Griffies, R. W. Hallberg, E. Shevliakova, *et al.*, "GFDL's ESM2 global coupled climate–carbon earth system models. Part I: Physical formulation and baseline simulation characteristics," *Journal of Climate,* vol. 25, pp. 6646-6665, 2012.

[92] U. S. F. E. M. Agency, *Design and Construction Guidance for Community Safe Rooms*: FEMA, 2008.

[93] R. A. Flather, "A numerical model investigation of tides and diurnal-period continental shelf waves along Vancouver Island," *Journal of Physical Oceanography,* vol. 18, pp. 115-139, 1988.

[94] R. A. Flather, "A storm surge prediction model for the northern Bay of Bengal with application to the cyclone disaster in April 1991," *Journal of Physical Oceanography,* vol. 24, pp. 172-190, 1994.

[95] H. J. Fowler, S. Blenkinsop, and C. Tebaldi, "Linking climate change modelling to impacts studies: recent advances in downscaling techniques for hydrological modelling," *International journal of climatology,* vol. 27, pp. 1547-1578, 2007.

[96] C. Frei, R. Schöll, S. Fukutome, J. Schmidli, and P. L. Vidale, "Future change of precipitation extremes in Europe: Intercomparison of scenarios from regional climate models," *Journal of Geophysical Research: Atmospheres,* vol. 111, 2006.

[97] J. Garratt, "Review of drag coefficients over oceans and continents," *Monthly weather review,* vol. 105, pp. 915-929, 1977.

[98] S. L. Gebre and F. Ludwig, "Hydrological response to climate change of the upper Blue Nile River Basin: based on IPCC Fifth Assessment Report (AR5)," *J Climatol Weather Forecasting,* vol. 3, p. 2, 2015.

[99] F. Giorgi, E. Coppola, F. Solmon, L. Mariotti, M. Sylla, X. Bi*, et al.*, "RegCM4: model description and preliminary tests over multiple CORDEX domains," *Climate Research,* vol. 52, pp. 7-29, 2012.

[100] H. C. Graber, V. J. Cardone, R. E. Jensen, D. N. Slinn, S. C. Hagen, A. T. Cox*, et al.*, "TROPICAL," *Oceanography,* vol. 19, p. 130, 2006.

[101] L. P. Graham, J. Andréasson, and B. Carlsson, "Assessing climate change impacts on hydrology from an ensemble of regional climate models, model scales and linking methods–a case study on the Lule River basin," *Climatic Change,* vol. 81, pp. 293-307, 2007.

[102] T. M. Hall and A. H. Sobel, "On the impact angle of Hurricane Sandy's New Jersey landfall," *Geophysical Research Letters,* vol. 40, pp. 2312-2315, 2013.

[103] S. Hallegatte, C. Green, R. J. Nicholls, and J. Corfee-Morlot, "Future flood losses in major coastal cities," *Nature climate change,* vol. 3, p. 802, 2013.

[104] A. F. Hamlet, P. W. Mote, M. P. Clark, and D. P. Lettenmaier, "Effects of temperature and precipitation variability on snowpack trends in the western United States," *Journal of Climate,* vol. 18, pp. 4545-4561, 2005.

[105] X. Hao, Y. Chen, C. Xu, and W. Li, "Impacts of climate change and human activities on the surface runoff in the Tarim River Basin over the last fifty years," *Water resources management,* vol. 22, pp. 1159-1171, 2008.

[106] I. M. Hartanto, L. Beevers, I. Popescu, and N. G. Wright, "Application of a coastal modelling code in fluvial environments," *Environmental modelling & software,* vol. 26, pp. 1685-1695, 2011.

[107] K. Hayhoe, C. Wake, B. Anderson, X.-Z. Liang, E. Maurer, J. Zhu*, et al.*, "Regional climate change projections for the Northeast USA," *Mitigation and Adaptation Strategies for Global Change,* vol. 13, pp. 425-436, 2008.

[108] S. Hempel, K. Frieler, L. Warszawski, J. Schewe, and F. Piontek, "A trend-preserving bias correction–the ISI-MIP approach," *Earth System Dynamics,* vol. 4, pp. 219-236, 2013.

[109] J. L. Hench, B. O. Blanton, and R. A. Luettich Jr, "Lateral dynamic analysis and classification of barotropic tidal inlets," *Continental Shelf Research,* vol. 22, pp. 2615-2631, 2002.

[110] Y. Hirabayashi, S. Kanae, S. Emori, T. Oki, and M. Kimoto, "Global projections of changing risks of floods and droughts in a changing climate," *Hydrological Sciences Journal,* vol. 53, pp. 754-772, 2008.

[111] G. D. Hubbert and K. L. Mclnnes, "A storm surge inundation model for coastal planning and impact studies," *Journal of Coastal Research,* pp. 168-185, 1999.

[112] K. F. Ahmed, G. Wang, J. Silander, A. M. Wilson, J. M. Allen, R. Horton, *et al.*, "Statistical downscaling and bias correction of climate model outputs for climate change impact assessment in the US northeast," *Global and Planetary Change,* vol. 100, pp. 320-332, 2013.

[113] K. E. Taylor, R. J. Stouffer, and G. A. Meehl, "An overview of CMIP5 and the experiment design," *Bulletin of the American Meteorological Society,* vol. 93, pp. 485-498, 2012.

[114] C. Tebaldi, B. H. Strauss, and C. E. Zervas, "Modelling sea level rise impacts on storm surges along US coasts," *Environmental Research Letters,* vol. 7, p. 014032, 2012.

[115] C. Teutschbein and J. Seibert, "Regional climate models for hydrological impact studies at the catchment scale: a review of recent modeling strategies," *Geography Compass,* vol. 4, pp. 834-860, 2010.

[116] C. Teutschbein and J. Seibert, "Bias correction of regional climate model simulations for hydrological climate-change impact studies: Review and evaluation of different methods," *Journal of Hydrology,* vol. 456, pp. 12-29, 2012.

[117] K. Trenberth, "Uncertainty in hurricanes and global warming," *Science,* vol. 308, pp. 1753-1754, 2005.

[118] E. Tsvetsinskaya, L. Mearns, T. Mavromatis, W. Gao, L. McDaniel, and M. Downton, "The effect of spatial scale of climatic change scenarios on simulated maize, winter wheat, and rice production in the southeastern United States," in *Issues in the Impacts of Climate Variability and Change on Agriculture*, ed: Springer, 2003, pp. 37-71.

[119] B. WBM, "TUFLOW User Manual-GIS Based 2D/1D Hydrodynamic Modelling," Report2008.

[120] J. J. van der Vegt and H. Van der Ven, "Space–time discontinuous Galerkin finite element method with dynamic grid motion for inviscid compressible flows: I. General formulation," *Journal of Computational Physics,* vol. 182, pp. 546-585, 2002.

[121] P. Vincent and C. Le Provost, "Semidiurnal tides in the northeast Atlantic from a finite element numerical model," *Journal of Geophysical Research: Oceans,* vol. 93, pp. 543-555, 1988.

[122] L. Warszawski, K. Frieler, V. Huber, F. Piontek, O. Serdeczny, and J. Schewe, "The inter-sectoral impact model intercomparison project (ISI–MIP): project framework," *Proceedings of the National Academy of Sciences,* vol. 111, pp. 3228-3232, 2014.

[123] S. Watanabe, T. Hajima, K. Sudo, T. Nagashima, T. Takemura, H. Okajima*, et al.*, "MIROC-ESM 2010: Model description and basic results of CMIP5-20c3m experiments," *Geoscientific Model Development,* vol. 4, p. 845, 2011.

[124] I. Watterson, J. Bathols, and C. Heady, "What influences the skill of climate models over the continents?," *Bulletin of the American Meteorological Society,* vol. 95, pp. 689-700, 2014.

[125] G. P. Weedon, G. Balsamo, N. Bellouin, S. Gomes, M. J. Best, and P. Viterbo, "The WFDEI meteorological forcing data set: WATCH Forcing Data methodology applied to ERA-Interim reanalysis data," *Water Resources Research,* vol. 50, pp. 7505-7514, 2014.

[126] G. Weedon, S. Gomes, P. Viterbo, W. Shuttleworth, E. Blyth, H. Österle*, et al.*, "Creation of the WATCH forcing data and its use to assess global and regional reference crop evaporation over land during the twentieth century," *Journal of Hydrometeorology,* vol. 12, pp. 823-848, 2011.

[127] M. Werner, "Impact of grid size in GIS based flood extent mapping using a 1D flow model," *Physics and Chemistry of the Earth, Part B: Hydrology, Oceans and Atmosphere,* vol. 26, pp. 517-522, 2001.

[128] P. Wessel and W. H. Smith, "A global, self-consistent, hierarchical, high-resolution shoreline database," *Journal of Geophysical Research: Solid Earth,* vol. 101, pp. 8741-8743, 1996.

[129] J. Westerink, R. Luettich Jr, C. Blain, and N. W. Scheffner, "ADCIRC: An Advanced Three-Dimensional Circulation Model for Shelves, Coasts, and Estuaries. Report 2. User's Manual for ADCIRC-2DDI," ARMY ENGINEER WATERWAYS EXPERIMENT STATION VICKSBURG MS1994.

[130] J. Westerink, R. Luettich, C. Blain, and S. Hagen, "Surface elevation and circulation in continental margin waters," ed: John Wiley & Sons, Inc., New York, New York, 1995, pp. 39-59.

[131] J. Westerink, R. Luettich, and J. Muccino, "Modelling tides in the western North Atlantic using unstructured graded grids," *Tellus A,* vol. 46, pp. 178-199, 1994.

[132] R. L. Wilby, S. Charles, E. Zorita, B. Timbal, P. Whetton, and L. Mearns, "Guidelines for use of climate scenarios developed from statistical downscaling methods," *Supporting material of the Intergovernmental Panel on Climate Change, available from the DDC of IPCC TGCIA,* vol. 27, pp. -, 2004.

[133] R. L. Wilby and T. Wigley, "Downscaling general circulation model output: a review of methods and limitations," *Progress in physical geography,* vol. 21, pp. 530-548, 1997.

[134] A. W. Wood, L. R. Leung, V. Sridhar, and D. Lettenmaier, "Hydrologic implications of dynamical and statistical approaches to downscaling climate model outputs," *Climatic change,* vol. 62, pp. 189-216, 2004.

[135] H.-C. Wu, M. K. Lindell, and C. S. Prater, "Logistics of hurricane evacuation in Hurricanes Katrina and Rita," *Transportation research part F: traffic psychology and behaviour,* vol. 15, pp. 445-461, 2012.

[136] C.-y. Xu, E. Widén, and S. Halldin, "Modelling hydrological consequences of climate change—progress and challenges," *Advances in Atmospheric Sciences,* vol. 22, pp. 789-797, 2005.

[137] Z. Yang and E. P. Myers, "Barotropic tidal energetics and tidal datums in the Gulf of Maine and Georges Bank region," in *Estuarine and Coastal Modeling (2007)*, ed, 2008, pp. 74-94.

[138] J. Yin, N. Lin, and D. Yu, "Coupled modeling of storm surge and coastal inundation: a case study in New York City during Hurricane Sandy," *Water Resources Research,* vol. 52, pp. 8685-8699, 2016.

[139] L. Zou and T. Zhou, "Near future (2016-40) summer precipitation changes over China as projected by a regional climate model (RCM) under the RCP8. 5 emissions scenario: Comparison between RCM downscaling and the driving GCM," *Advances in Atmospheric Sciences,* vol. 30, pp. 806-818, 2013.